

## ON THE EVOLUTIONARY AND PULSATION MASS OF CLASSICAL CEPHEIDS: III. THE CASE OF THE ECLIPSING BINARY CEPHEID CEP0227 IN THE LARGE MAGELLANIC CLOUD

P. G. PRADA MORONI<sup>1,2</sup>, M. GENNARO<sup>3</sup>, G. BONO<sup>4,5</sup>, G. PIETRZYŃSKI<sup>6,7</sup>, W. GIEREN<sup>6</sup>, B. PILECKI<sup>6,7</sup>, D. GRACZYK<sup>6</sup>, I. B. THOMPSON<sup>8</sup>

*Draft version November 1, 2018*

### ABSTRACT

We present a new Bayesian approach to constrain the intrinsic parameters (stellar mass, age) of the eclipsing binary system –CEP0227– in the Large Magellanic Cloud. We computed several sets of evolutionary models covering a broad range in chemical compositions and in stellar mass. Independent sets of models were also constructed either by neglecting or by including a moderate convective core overshooting ( $\beta_{ov}=0.2$ ) during central hydrogen burning phases. Sets of models were also constructed either by neglecting or by assuming a canonical ( $\eta=0.4,0.8$ ) or an enhanced ( $\eta=4$ ) mass loss rate. The most probable solutions were computed in three different planes: luminosity–temperature, mass–radius and gravity–temperature. By using the Bayes Factor, we found that the most probable solutions were obtained in the gravity–temperature plane with a Gaussian mass prior distribution. The evolutionary models constructed by assuming a moderate convective core overshooting ( $\beta_{ov}=0.2$ ) and a canonical mass loss rate ( $\eta=0.4$ ) give stellar masses for the primary (Cepheid) – $M=4.14^{+0.04}_{-0.05} M_{\odot}$ – and for the secondary – $M=4.15^{+0.04}_{-0.05} M_{\odot}$ – that agree at the 1% level with dynamical measurements. Moreover, we found ages for the two components and for the combined system – $t=151^{+4}_{-3}$  Myr– that agree at the 5% level. The solutions based on evolutionary models that neglect the mass loss attain similar parameters, while those ones based on models that either account for an enhanced mass loss or neglect convective core overshooting have lower Bayes Factors and larger confidence intervals. The dependence on the mass loss rate might be the consequence of the crude approximation we use to mimic this phenomenon.

By using the isochrone of the most probable solution and a Gaussian prior on the LMC distance, we found a true distance modulus – $18.53^{+0.02}_{-0.02}$  mag– and a reddening value – $E(B-V)=0.142^{+0.005}_{-0.010}$  mag– that agree quite well with similar estimates in the literature.

*Subject headings:* stars: classical Cepheids — stars: evolution — stars: oscillations — stars: fundamental parameters

### 1. INTRODUCTION

Classical Cepheids are very popular in the recent literature, since they play a crucial role to address several open astrophysical problems. The reason is threefold. *i)*– They are the most popular primary distance indicators, since they are bright and can be easily identified. *ii)*– They are excellent tracers of intermediate-mass stars, since their evolutionary status is well defined (central helium burning, blue loops). *iii)*– They are fundamental laboratories to constrain the micro (equation of state, opacity, cross sections) and macro (mass loss, mixing, convective transport) physics adopted in both evolutionary and pulsation models.

Dating back to the seminal investigation by Hofmeister, Kippenhahn & Weigert (1964, and references therein) and by Becker & Iben (1979), the evolutionary properties of intermediate-mass have been investigated in a series of theoretical (Stothers & Chin 1978; Chiosi & Maeder 1986; Castellani, Chieffi & Straniero 1990; Langer 1991; Bono et al. 2000; Maeder & Meynet 2000; Meynet & Maeder 2002; Karakas & Lattanzio 2003; Pietrinferni et al. 2004, 2006; Valle et al. 2009; Charbonnel & Lagarde 2010; Cassisi & Salaris 2011; Neilson, Cantiello, & Langer 2011; Brott et al. 2011a,b) and empirical (Alcock et al. 1999; Testa et al. 1999; Brocato et al. 2003; Hunter et al. 2009a,b; Bonanos et al. 2009, 2010; Sanna et al. 2009; Efremova et al. 2011) investigations.

One of the most interesting problem concerning evolutionary and pulsation properties of classical Cepheids is the so-called mass discrepancy problem. During the late sixties it was noticed by Christy (1966, 1970) and by Stobie (1969) that the evolutionary masses –estimated using the comparison between isochrones and observations in the Color-Magnitude Diagram (CMD)– were almost a factor of two larger than the pulsation masses –estimated using the Period-Mass-Radius relation– of Galactic Cepheids (Fricke, Stobie, & Strittmatter 1971).

This conundrum was partially solved by

<sup>1</sup> Dipartimento di Fisica, Università di Pisa, Largo B. Pontecorvo 2, 56127 Pisa, Italy; prada@df.unipi.it

<sup>2</sup> INFN–Pisa, via E. Fermi 2, 56127 Pisa, Italy

<sup>3</sup> Max-Planck-Institut für Astronomie, Königstuhl 17, D-69117, Heidelberg, Germany

<sup>4</sup> Dipartimento di Fisica, Università di Roma Tor Vergata, Via della Ricerca Scientifica 1, 00133 Roma, Italy

<sup>5</sup> INAF–Osservatorio Astronomico di Roma, Via Frascati 33, 00040 Monte Porzio Catone, Italy

<sup>6</sup> Universidad de Concepción, Departamento de Astronomía, Casilla 160-C, Concepción, Chile

<sup>7</sup> Obserwatorium Astronomiczne Uniwersytetu Warszawskiego, Aleje Ujazdowskie 4, 00-478 Warszawa, Poland

<sup>8</sup> Carnegie Observatories, 813 Santa Barbara Street, Pasadena, CA 91101-1292, USA

Moskalik, Buchler, & Marom (1992) using the sets of radiative opacities released by the OPAL (Iglesias & Rogers 1991) and by the Opacity Project (Seaton et al. 1994) groups. However, several investigations focussed on Galactic (Bono et al. 2001; Caputo et al. 2005)) and Magellanic (Beaulieu, Buchler, & Kollath 2001; Bono et al. 2002; Keller & Wood 2002, 2006; Keller 2006) Cepheids suggested that such a discrepancy was still of the order of 10-20%. A similar discrepancy was also found by Evans et al. (2005a) using dynamical mass estimates of Galactic binary Cepheids and by Brocato et al. (2003) using cluster Cepheids located in NGC 1866, a young Large Magellanic Cloud (LMC) cluster.

The Cepheid mass discrepancy problem can be addressed following two different paths.

*a) –He-core mass–* current evolutionary predictions underestimate the He-core mass for intermediate-mass structures, and in turn their Mass-Luminosity (ML) ratio. This possible drawback has a substantial impact both on evolutionary and pulsation predictions, since the latter models assume an ML relation.

*b) –Envelope mass–* Current Cepheid masses are smaller than their main sequence (MS) progenitors, because they have lost a fraction of their initial envelope mass. The latter working hypothesis implies that the Cepheid mass discrepancy is intrinsic, i.e., it is not caused by limits in the physical assumptions adopted in constructing evolutionary and pulsation models. The input physics adopted in constructing evolutionary models of intermediate-mass stars has already been addressed in several papers (Chiosi & Maeder 1986; Brocato & Castellani 1993; Stothers & Chin 1993, 1996; Cassisi et al. 2004; Bertelli et al. 2009; Valle et al. 2009).

Here, we briefly mention the most relevant ones affecting the He-core mass and the envelope mass.

*a) He-core mass*

*i) –Extra-mixing–* Several detailed studies based on the comparison between predicted CMDs and Luminosity Functions of NGC1866, reached opposite conclusions in favor (Barmina, Girardi, & Chiosi 2002) and against (Testa et al. 1999; Brocato et al. 2003) the occurrence of mild convective core overshooting. The need for a mild overshooting was also suggested by Keller & Wood (2006) who investigated several young clusters in the LMC and in the Small Magellanic Cloud. More recently, it has also been suggested by Cordier et al. (2002) that the degree of overshooting might also depend on the metal abundance, namely it increases when metal abundance decreases. *ii) –Rotation–* Evolutionary models constructed by accounting for the effects of rotation predict both an increase in Helium core mass and an enhancement in the surface abundance of both Helium and Nitrogen (Meynet & Maeder 2002). It has also been suggested that rotation might account for the significant changes in surface chemical compositions observed in Galactic and Magellanic supergiants (Korn et al. 2005; Hunter et al. 2009a,b). Moreover, recent theoretical (Maeder & Meynet 2000) and empirical (Venn 1999) investigations indicate that the efficiency of such a mechanism might depend on the initial metal abundance, i.e., it increases when metal abundance decreases. *iii) –Radiative Opacity–* A new set of radiative opacities

has been recently computed by the Opacity Project (Badnell et al. 2005). The difference between old and new opacities is at most of the order of 5-10% across the Z-bump ( $T \approx 250,000$  K). To account for the mass discrepancy the increase in the opacity should be almost a factor of two. This indicates that the adopted radiative opacities have a marginal impact on the mass discrepancy problem.

*b) Envelope mass*

*i) –Canonical Mass Loss–* The total mass of an actual Cepheid is also affected by a decrease in the envelope mass. Evolutionary models accounting for the mass loss, during Hydrogen and Helium burning phases, by means of several semi-empirical relations (Reimers 1975; Nieuwenhuijzen & de Jager 1990) do not solve the Cepheid mass discrepancy problem. Plausible values for the free parameter  $-\eta$  give mass loss rates that are too small. This is not surprising, since current semi-empirical relations are only based on scaling arguments and they are not rooted on a robust physical basis (Schroeder & Cuntz 2005). Empirical mass loss estimates based on NIR and ultraviolet emission for Galactic (McAlary & Welch 1986; Deasy 1988; Marengo et al. 2010a) and Large Magellanic Cloud (Neilson & Lester 2008; Neilson et al. 2009) Cepheids cover a broad range ( $10^{-10} - 10^{-7} M_{\odot} \text{ yr}^{-1}$ ). *ii) –Enhanced Mass Loss–* More recent mid-infrared observations for 29 Galactic Cepheids collected with Spitzer indicate the presence of extended emission around seven of them (Barmby et al. 2011). This finding together with the interferometric detection of circumstellar shells around several Galactic Cepheids (Merand et al. 2006, 2007; Kervella et al. 2006, 2008; Kervella, Merand & Gallenne 2009) further supports the evidence that there is a wind associated with Cepheids possibly triggered by pulsation-driven mass loss.

A new spin concerning the occurrence of circumstellar shells around Cepheids was recently given by the detection of a large nebula around  $\delta$  Cephei (Marengo et al. 2010b), the prototype of Cepheid variables. The IR emission was detected in several MIR bands and shows a radial extent larger than  $10^4$  AU (5 arcmin). The nebula shows a parabolic shape and it is aligned with the direction of the motion, thus suggesting the possible occurrence of a bow shock caused by the interaction between the mass-losing Cepheid with the interstellar material. Current estimates indicate that  $\delta$  Cephei may be losing mass with a rate of  $\sim 5 \times 10^{-9}$  to  $\sim 6 \times 10^{-8} M_{\odot} \text{ yr}^{-1}$ . This finding has been independently confirmed by Matthews et al. (2011) using data collected in the radio with the Extended Very Large Array. They found an outflow velocity of  $\sim 36$  km/s and a mass loss rate of  $\sim 10^{-7} - 10^{-6} M_{\odot} \text{ yr}^{-1}$ . The modest dust content of the outflow indicates that the wind from  $\delta$  Cephei might be pulsation-driven instead of dust-driven as typical for other classes of evolved stars.

However, the stepping stone concerning the evolutionary and pulsation properties of classical Cepheids was the detection of a Cepheid in a well detached, double-lined eclipsing binary system in the Large Magellanic Cloud. The geometry and the precision of both photometric and spectroscopic data gave the opportunity to measure the

mass of the Cepheid (CEP0227) with the unprecedented precision of 1% (Pietrzynski et al. 2010, hereinafter Paper I). A similar precision was also attained for the classical Cepheid in the LMC eclipsing binary CEP1812 by (Pietrzynski et al. 2011, hereinafter Paper II).

This finding paved the road for new constraints on pulsation and evolutionary masses. Soon after, Cassisi & Salaris (2011) by using evolutionary models that account for a moderate convective core overshooting found evolutionary masses agree quite well with the dynamical mass of CEP0227 both in the Radius-Age plane and in the Radius-Effective Temperature plane. More recently, Neilson, Cantiello, & Langer (2011) found that a combination of both moderate convective core overshooting and pulsation-driven mass loss is required to solve the Cepheid mass discrepancy.

This is the third paper of a series focussed on the evolutionary and pulsation properties of Cepheids. The new series present two novel approaches when compared with similar investigations available in the literature: *i)*– the intrinsic parameters will be estimated using a Bayesian approach in dealing with the comparison between theory and observations; *ii)*– the empirical measurements are based on a homogeneous approach for both photometry and spectroscopy. In this investigation we provide new evolutionary constraints on the binary Cepheid CEP0227.

The plan of the paper is the following. In §2 we introduce the input physics adopted to construct evolutionary models. We also discuss the physical assumptions adopted to deal with mass loss, mixing and convective transport. In this section, we also outline the assumptions adopted to compute stellar isochrones. The description of the method adopted to estimate the intrinsic parameters of the binary components is given in §3. In this section we discuss the different most probable solutions in the L–T, in the M–R and in the g–T planes. §4 deals with the new empirical constraints on both stellar mass and age we obtained in the different planes for the binary system. In §5 we address the comparison between the most probable stellar isochrone and observations in the Color-Magnitude diagram. The true distance modulus and the reddening for the combined system are also discussed. In §6 we summarize the results and outline future possible avenues of the project.

## 2. THE THEORETICAL FRAMEWORK

### 2.1. *Input physics*

The evolutionary tracks were computed with an updated version of the FRANEC evolutionary code (Degl’Innocenti et al. 2008; Valle et al. 2009; Tognelli, Prada Moroni, & Degl’Innocenti 2011; Dell’Omodarme et al. 2011). For these models, the 2006 release of the OPAL equation of state (EOS) was adopted (Rogers et al. 1996), together with the radiative opacity tables released in 2005 by the same Livermore group (Iglesias & Rogers 1996)<sup>9</sup> for  $\log T[K] > 4.5$  and extended at lower temperatures with the radiative opacity tables by Ferguson et al. (2005). The conductive opacities are from Shternin & Yakovlev (2006, see also Potekhin (1999)). All the opacity tables were

calculated for the Asplund et al. (2009, hereafter As09) heavy-element solar mixture. The nuclear reaction rates are from the NACRE compilation (Angulo et al. 1999), except for the  $^{14}\text{N}(p,\gamma)^{15}\text{O}$ , which is from the LUNA collaboration (Imbriani et al. 2005; Bemmerer et al. 2006; Lemut et al. 2006) and  $^{12}\text{C}(\alpha,\gamma)^{16}\text{O}$  from Hammer et al. (2005). These two reactions (see, e.g., Valle et al. 2009, and references therein) affect both the extension and the morphology of the loop performed by intermediate-mass He-burning stars in the HR diagram. Hence the most recent values should always be adopted in stellar evolutionary codes in order to provide reliable theoretical predictions.

Current calculations did not take into account He and metal diffusion, since its effect on the evolutionary properties of intermediate-mass stars is minimal. To model super-adiabatic convection, we adopted the mixing-length formalism (Böhm-Vitense 1958), in which the efficiency of the convective transport depends on the mixing-length, i.e.  $l = \alpha H_p$ , where  $H_p$  is the pressure height-scale and  $\alpha$  is a free parameter. The  $\alpha$  value – 1.74 – was calibrated using the Standard Solar Models computed with both the same code and the same input physics, in particular using the same heavy-element mixture (As09). To account for current theoretical and empirical uncertainties, additional models with  $\alpha=1.9$  were also computed. We also account for convective core overshooting, during central hydrogen burning phases, by extending the central mixed region of  $l_{ov}=\beta H_p$  from the border of the standard convective core defined by the Schwarzschild criterion, where  $\beta$  is a free parameter (Castellani et al. 2000; Valle et al. 2009). Note that we do not account for a mechanical core overshooting during the central He-burning phase. The use of the Schwarzschild criterion to determine the convective core extension, during these phases, would lead to an unphysical discontinuity in the radiative gradient at the border of the convective core. This effect is caused by the increase in the opacity due to the conversion of He into C and O (Cassisi et al. 2004). To overcome the problem we model the growth of the convective core and the development of a semiconvective region following Castellani et al. (1971a,b). Note that we neglect the convective overshooting at the base of the convective envelope during shell hydrogen burning phases.

### 2.2. *Evolutionary tracks*

The approach we plan to adopt to estimate the intrinsic parameters of the binary components does require detailed set of evolutionary tracks and of isochrones properly covering the helium burning phases. The stellar masses of the evolutionary tracks range from 3 to 5  $M_\odot$ , and the step in stellar mass is 0.05  $M_\odot$ . Therefore, each set includes 42 evolutionary tracks. Unfortunately, we still lack an accurate measurement of the iron and heavy element abundances of CEP0227. Therefore, we adopted the mean metallicity of LMC Cepheids ( $[\text{Fe}/\text{H}]=-0.33\pm 0.13$  dex) based on recent high-resolution, high signal-to-noise spectra collected with UVES at ESO/VLT (Romaniello et al. 2008). The top, left panel of Fig. 1 shows the set of evolutionary models computed at fixed helium ( $Y=0.260$ ) and metal ( $Z=0.006$ ) content and stellar masses ranging from 3 to

<sup>9</sup> <http://opalopacity.llnl.gov/opal.html>.

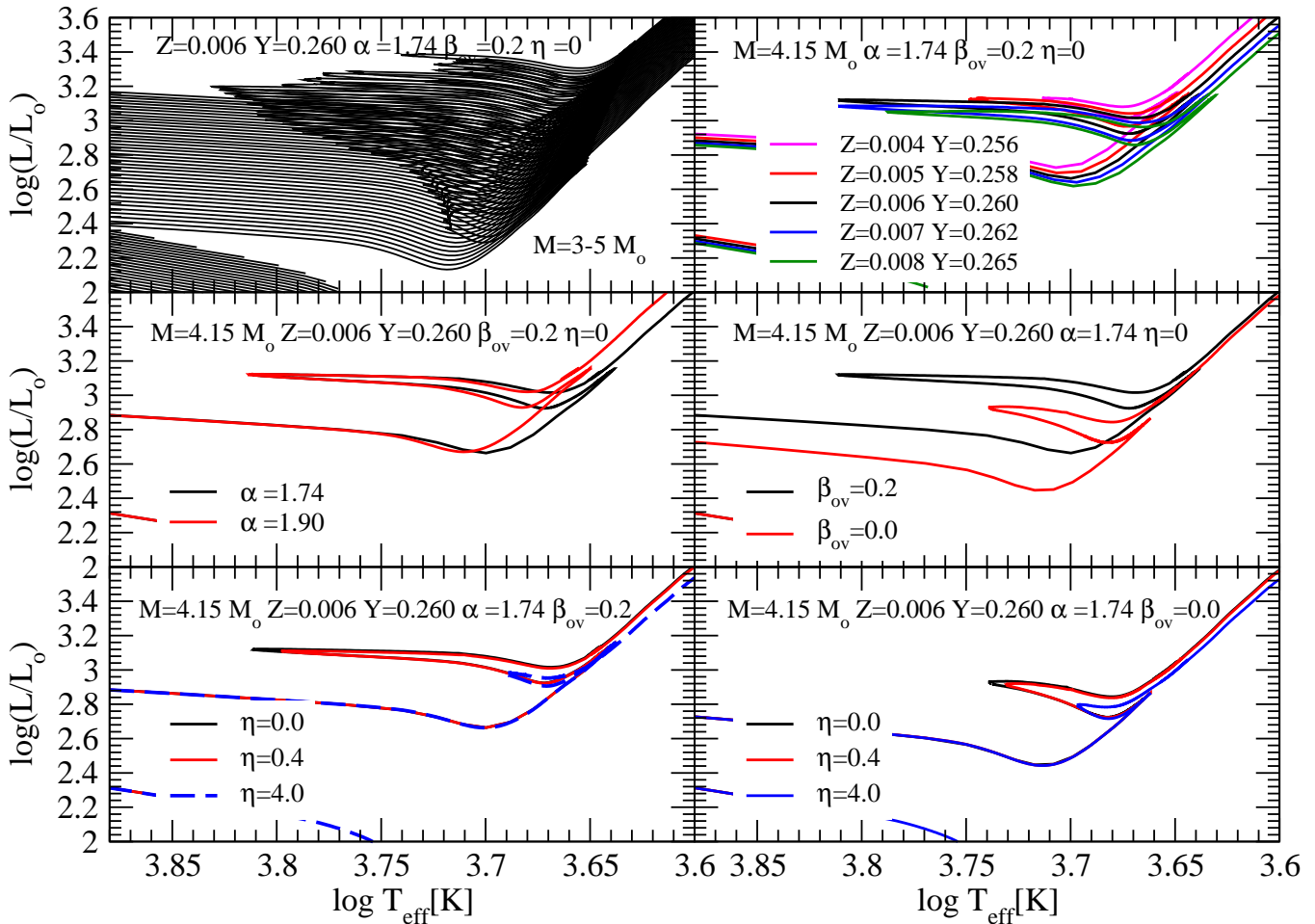


FIG. 1.— Top – Left – Hertzsprung-Russell Diagram of a set of evolutionary tracks computed at fixed metal ( $Z=0.006$ ) and helium ( $Y=0.260$ ) abundance and stellar masses ranging from 3 to 5  $M_{\odot}$ . The plot is focussed around the evolutionary phases of central helium burning (blue loops). The free parameters adopted to deal with convective transport (mixing length,  $\alpha$ ), with convective core overshooting ( $\beta$ ) and with mass loss ( $\eta$ ) are also labeled. Top – Right – Same as the Top-Left, but for evolutionary tracks computed at fixed stellar mass ( $M=4.15 M_{\odot}$ ), but different chemical compositions (see labeled values). Middle – Left – Same as the Top-Left, but for evolutionary tracks computed at fixed stellar mass ( $M=4.15 M_{\odot}$ ) and chemical composition ( $Z=0.006$ ,  $Y=0.260$ ), but for two different assumptions concerning the mixing length (see labeled values). Middle – Right – Same as the Top-Left, but for evolutionary tracks computed at fixed stellar mass ( $M=4.15 M_{\odot}$ ) and chemical composition, but for two different assumptions concerning the convective core overshooting. Bottom – Left – Same as the Top-Left, but for evolutionary tracks computed at fixed stellar mass ( $M=4.15 M_{\odot}$ ) and chemical composition, but for three different assumptions concerning the mass loss rate. Bottom – Right – Same as the Bottom-Left, but for evolutionary tracks computed neglecting the convective core overshooting.

5  $M_{\odot}$ . The evolutionary phases plotted in this panel cover the central helium burning evolutionary phases (blue loops).

To take into account possible changes in iron abundance, due to intrinsic metallicity dispersion (Pompeia et al. 2008; Romaniello et al. 2008; Hunter et al. 2009a,b) we also computed four independent sets of evolutionary tracks with metallicity ranging from  $Z=0.004$  to  $Z=0.008$ , while the helium content was fixed assuming an helium-to-metal enrichment ratio  $\Delta Y/\Delta Z=2$  (Pagel & Portinari 1998; Jimenez et al. 2003; Flynn 2004; Gennaro, Prada Moroni, & Degl’Innocenti 2010) and a primordial helium abundance of  $Y_p=0.2485$  (see, e.g., Cyburt et al. 2005; Steigman 2006; Peimbert, Luridiana, & Peimbert 2007; Komatsu et al. 2011). Therefore, current helium values range from  $Y=0.256$  to  $Y=0.265$  (see top, right panel of Fig. 1).

We already mentioned that intermediate-mass stars are

affected by uncertainties on the actual size of the He-core mass. To constrain the impact of the convective core overshooting during central hydrogen burning phases on the intrinsic parameters, the evolutionary tracks were computed either neglecting ( $\beta_{ov}=0$ ) or accounting for a moderate convective core overshooting ( $\beta_{ov}=0.2$ , see top panels of Fig. 1). The two components of the binary system are relatively cool objects (see Table 1) with extended convective envelopes. To constrain the dependence on the efficiency of convective transport in the super-adiabatic regions the calculations were performed assuming two different mixing length parameters. The former one  $-\alpha=1.74$ – calibrated using the standard solar model (Dell’Omodarme et al. 2011) and the latter one  $-\alpha=1.90$ – to mimic a more efficient convection (see middle panels of Fig. 1).

Recent theoretical investigations based on evolutionary models accounting for both convective core overshooting and for a pulsation driven mass loss suggested

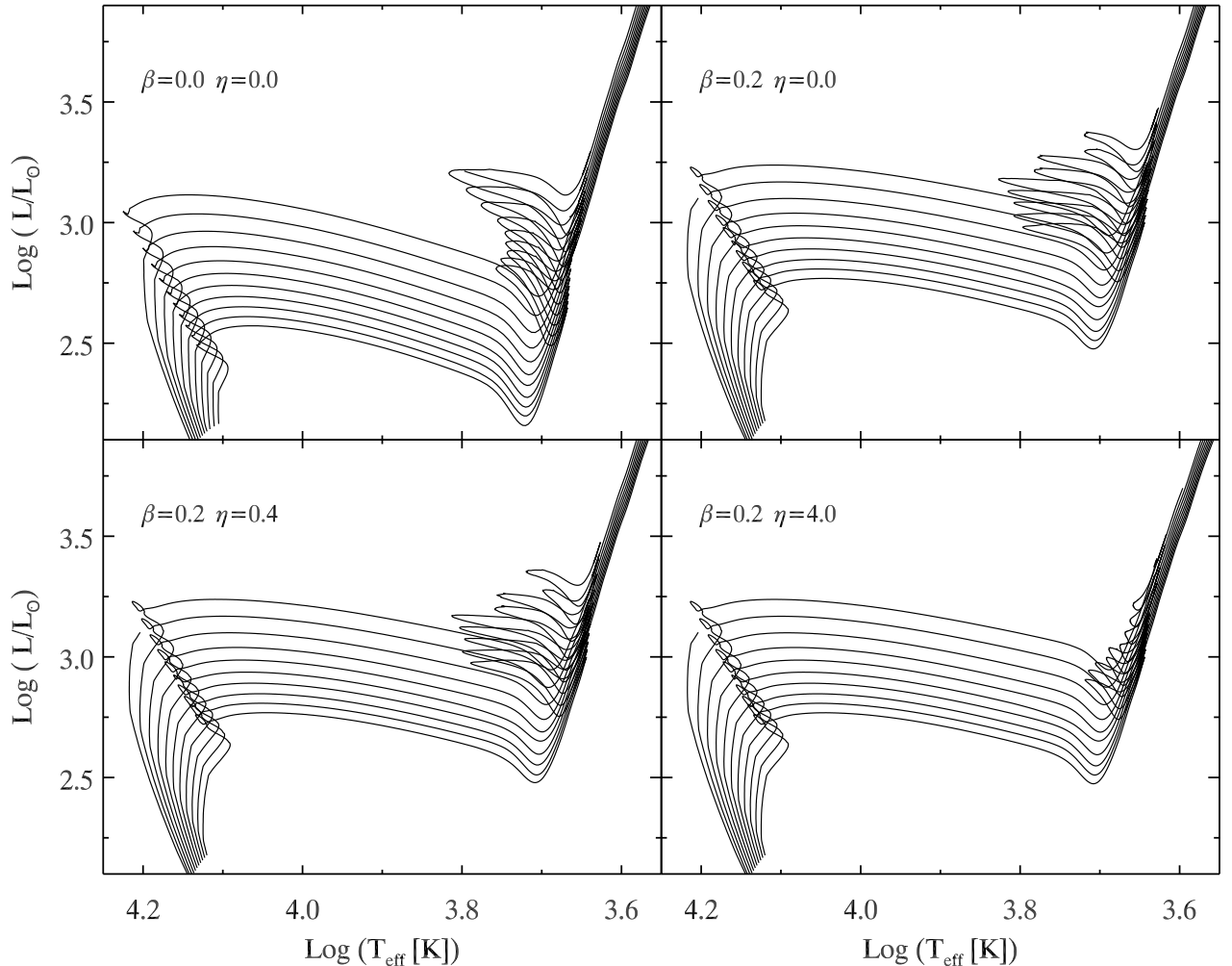


FIG. 2.— Hertzsprung-Russell Diagram of sets of isochrones computed at fixed metal ( $Z=0.006$ ) and helium ( $Y=0.260$ ) abundance and ages ranging from 80 to 180 Myr, with a step in age of 10 Myr.

that the latter physical mechanism can play a crucial role in settling the Cepheid mass discrepancy problem (Neilson, Cantiello, & Langer 2011). A detailed analysis of the dependence of the blue loops on this physical mechanism is out of the aim of this investigation. However, to constrain the dependence of the most probable solution on the mass loss rate, different sets of evolutionary models were computed accounting for mass loss after the central hydrogen exhaustion. We used the Reimers formula

$$dM/dt = \eta \times 4 \times 10^{-13} \times L/gR \quad [M_{\odot}/\text{yr}]$$

where  $\eta$  is a free parameter,  $L, R$  and  $g$  are the luminosity, the radius, and the surface gravity in solar units. Sets of models with four different  $\eta$  values, namely 0, 0.4, 0.8 and 4.0, were computed. The evolutionary tracks constructed by assuming  $\eta=0.4$  and 0.8 show marginal changes and in the following we will only take into account the former ones (see bottom panels of Fig. 1).

We ended up with a sample of more than 2,000 evolutionary tracks computed for this specific project.

### 2.3. Stellar isochrones

For each set of evolutionary tracks discussed in §2.2, we also computed a fine grid of stellar isochrones with ages ranging from a few tens to a few hundreds of Myr. To improve the accuracy of the parameter estimates (see §3) and to provide robust determinations of the confidence interval, the isochrones were further interpolated. The actual grid of isochrones has a step in age of 0.02 Myr, necessary to cover the fast evolution of the stars across the blue loop.

Subsets of isochrones for selected input parameters (see labeled values) in the HR diagram are shown in Fig.2.1.

### 3. PARAMETER ESTIMATES

The parameters that determine the evolutionary status of a star are its mass,  $\mu$ , its age,  $\tau$  and its chemical composition,  $\zeta$ . The value of these parameters determine the position of a star in the HR diagram or, similarly, in any diagram where observable properties are displayed. Stellar models predict observables as a function of these three parameters, hence their values can be estimated by comparing predictions and observations. To provide robust estimates of both stellar masses and ages of the binary components we followed the Bayesian approach

described in Gennaro, Prada Moroni, & Tognelli (2012). The interested reader is referred to the quoted paper, here we only summarize the relevant points of the approach we adopted.

### 3.1. Bayesian approach

Given a set of observables  $\vec{q}$  the probability of the model parameters,  $\vec{p} = (\mu, \tau, \zeta)$  is given by:

$$f(\vec{p}|\vec{q}) \propto \mathcal{L}(\vec{p}|\vec{q})f(\vec{p}). \quad (1)$$

Here  $\mathcal{L}(\vec{p}|\vec{q})$  is the Likelihood of the parameters  $\vec{p}$  given the set of observations  $\vec{q}$  and  $f(\vec{p})$  is the prior distribution of the parameters.

We used three different pairs of observables,  $\vec{q}$ , to determine the  $(\mu, \tau, \zeta)$  set of parameters of the binary components. In particular, we performed the comparison in the  $\vec{q} = (\log L/L_\odot, \log T_{\text{eff}}), (M/M_\odot, R/R_\odot)$  and  $(\log T_{\text{eff}}, \log g)$  planes.

To estimate the best values of the stellar masses and ages the probability  $f(\vec{p}|\vec{q})$  is marginalized w.r.t the other two variables:

$$G(\tau) = \int \mathcal{L}(\tau, \mu, \zeta|\vec{q})f(\tau, \mu, \zeta) d\mu d\zeta \quad (2)$$

$$H(\mu) = \int \mathcal{L}(\tau, \mu, \zeta|\vec{q})f(\tau, \mu, \zeta) d\tau d\zeta \quad (3)$$

The mode of the marginal distributions is used as the best parameter estimator (Jorgensen & Lindegren 2005; Gennaro, Prada Moroni, & Tognelli 2012). Confidence intervals are defined by excluding 16% of the area under the posterior distribution on each side of the variable domains.

In our treatment the metallicity is not considered as an unknown parameter to be determined. On the contrary, we adopted the available prior information on the metallicity of Cepheids in the LMC to constrain our predictions on the stellar masses and ages. In detail, we adopted a Gaussian distribution of  $[\text{Fe}/\text{H}]$  with mean  $\langle [\text{Fe}/\text{H}] \rangle = -0.33$  and standard deviation  $\sigma_{[\text{Fe}/\text{H}]} = 0.13$  dex. The quoted values are based on the metallicity distribution of LMC Cepheids measured by Romaniello et al. (2008).

Given the available information on the dynamical stellar masses we adopted two different priors for the stellar mass. In one case a flat prior is adopted, defined across the entire range of stellar masses for which we computed evolutionary tracks:  $M \in [3, 5]M_\odot$ . In the second case we used a prior with a Gaussian distribution with mean and standard deviations based on the dynamical mass estimates by Pietrzynski et al. (2010).

Stellar ages were estimated separately for the two binary components and for the system as a whole. The age of each star is determined from the  $G(\tau)$  marginal distribution of equation (2). In the reasonable hypothesis that the two components of the binary system have the same age, their composite age distribution, i.e. the age of the system, can be simply derived as:

$$G_C = G_P \times G_S; \quad (4)$$

where the subscripts indicate the composite (C), the primary component (P) and the secondary component (S) age distributions. In a recent investigation,

Gennaro, Prada Moroni, & Tognelli (2012) showed that the age distribution of a stellar system based on this approach is a more precise indicator of the real age when compared to single stellar ages.

The above approach was applied to each set of evolutionary models listed in Table 1, i.e. for each different assumption concerning the value of the overshooting parameter  $-\beta$ – the mass-loss  $-\eta$ – and the mixing length  $-\alpha$ – parameter. The posterior probabilities were computed using both the flat and the Gaussian prior on the stellar mass. Selected results of the individual solutions are given in Table 3. The solutions based on different observables are discussed in the following subsections.

### 3.2. The Hertzsprung-Russell Diagram

As a first step to constrain the intrinsic parameters of the binary system, we applied our method in the Hertzsprung-Russell Diagram. The main advantage in using this plane is that we can estimate the intrinsic luminosities using the Stefan-Boltzmann relation. Therefore, the solution is independent of distance modulus, reddening and stellar mass. The main drawback is that the two parameters (luminosity and temperature) are correlated and more affected by measurement errors than the stellar mass and the radius (see Fig. 3). However, our method takes into account the fact that temperature and luminosity are not independent, and indeed the covariance matrix is also included in the solution (see equations (3), (4) and (5) in Gennaro, Prada Moroni, & Tognelli 2012).

### 3.3. The stellar mass vs radius plane

To further constrain the intrinsic parameters of the binary system we also applied the Bayesian method in the stellar mass vs radius plane. The main advantage in using this plane is that the adopted observables are independent of distance modulus and reddening and they are also independent from each other (see Fig. 4).

### 3.4. The $\log T_{\text{eff}}$ vs $\log g$ plane

Finally, we applied the Bayesian method also into the effective temperature vs surface gravity plane. The main advantage in using this plane is that the adopted observables are independent of distance modulus and reddening. Moreover, the observables are independent from each other and the isochrones display a relevant difference in this age range (see Fig. 5). This plane combines three independent measurements, thus providing the most stringent test for the theory.

## 4. CONSTRAINTS ON THE STELLAR MASS AND AGE OF THE BINARY SYSTEM

The most probable mass and age values that we found indicate that the mixing length parameter has a minimal impact on the estimate of these parameters. This result is not surprising, since the extent in effective temperature of the blue loop is minimally affected by the change in  $\alpha$  from 1.74 to 1.90. This is the reason why in Table 3 we only included the results based on models with  $\alpha=1.74$ . What is clear from the values listed in Table 3 is that the solutions based on evolutionary models that do not account for the convective core overshooting and those with enhanced mass-loss ( $\eta = 4.0$ ) are in worse agreement with the measured dynamical masses, when

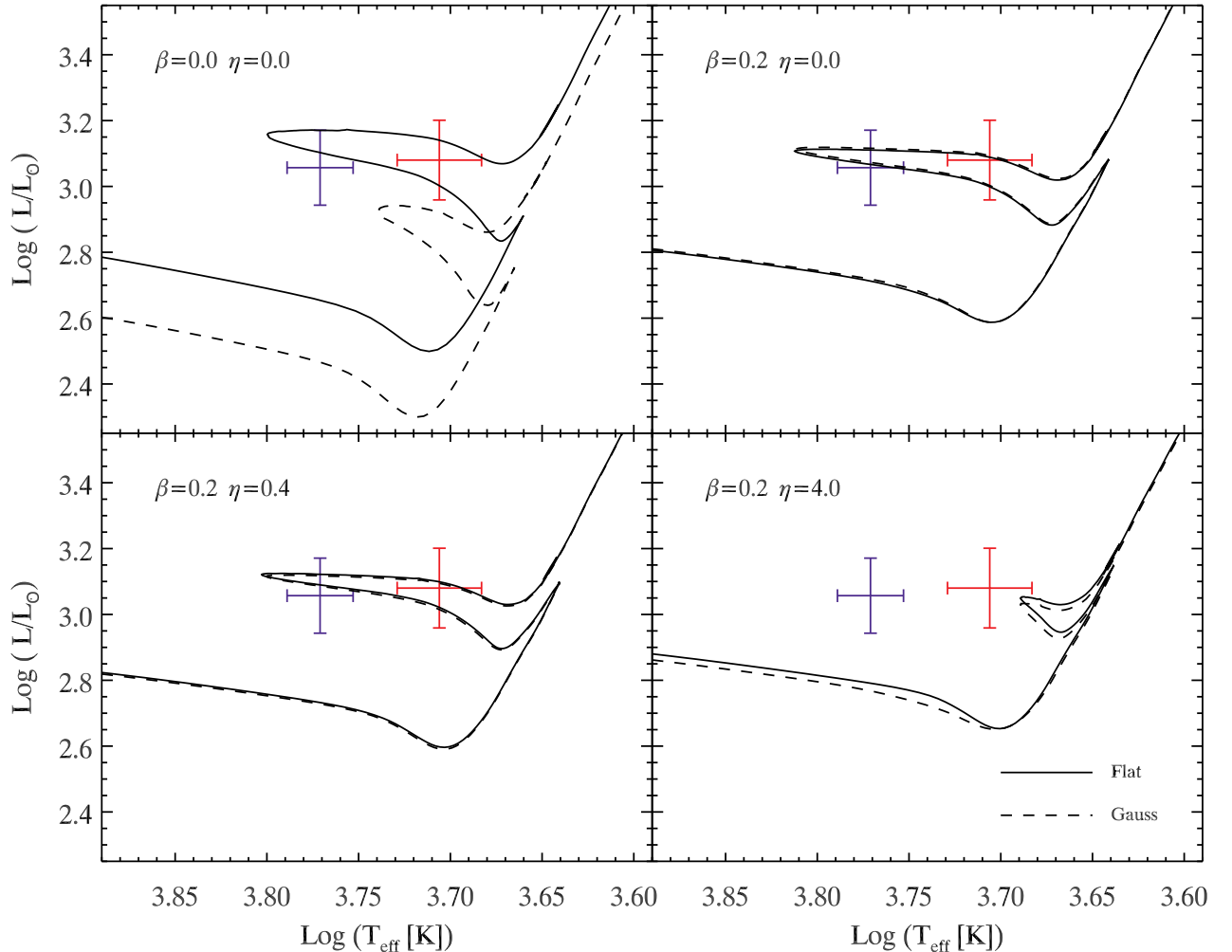


FIG. 3.— Top – Left– Comparison in the Hertzsprung-Russell Diagram between the binary components and the isochrone giving the maximum of  $G_C = G_P \times G_S$  (see Table 3). In this panel the solution is based on evolutionary models constructed by neglecting convective core overshooting ( $\beta=0$ ) and mass loss ( $\eta=0$ ). The solid and the dashed lines show the isochrones with most probable age derived using the Gaussian and the flat prior on the mass distribution, respectively. The blue bar marks the position of the Cepheid (primary), while the red ones the position of the red giant (secondary). The intrinsic parameters of the isochrones are also labeled. Top – Right– Same as top left, but for models accounting for mild ( $\beta=0.2$ ) convective core overshooting. Bottom – Same as the top right, but for models accounting for a canonical (left,  $\eta=0.4$ ) and an enhanced (right,  $\eta=4.0$ ) mass loss rate.

compared with the results based on models accounting for the convective core overshooting and  $\eta = 0.0$  or  $0.4$ .

In the case of a flat mass prior, the  $\beta = 0.0$  models predict stellar masses that are systematically larger than observed, even though the difference with the dynamical mass is typically within the  $1\sigma$  confidence interval. Similarly, the models with enhanced mass-loss, in the case of flat mass prior, tend to underestimate the mass of the primary component. These two sets of models give a good agreement with the data, only when the method is used in the M–R plane.

Comparing the results for a flat and a Gaussian mass prior, it is clear that the latter drives the solution towards the measured dynamical mass. While this might appear obvious, we will show in Sect. 4.1 that not only the mode of the mass distributions are shifted towards the measured values, but also the whole solution has a higher reliability, measured using the so-called evidence parameter (see §4.1). The impact of the Gaussian prior is

very important also for the age results. In the Gaussian mass prior case, the age solutions for the two components are generally more precise, meaning that the uncertainty interval is narrower compared to the flat prior case. In addition to this, there is also a better agreement between the ages of the two components, and therefore, a more robust result for the composite age of the system.

For each set of models, we plotted the isochrones corresponding to the most probable composite age (indicated by a C in Table 3) in Figs. 3, 4 and 5. The three figures show the most probable isochrone as obtained by applying the method in the L–T, in the M–R and in the g–T plane. Solid and dashed lines display the most probable ages for a flat and a Gaussian mass prior, respectively.

In passing, we note that evolutionary models constructed assuming a slightly enhanced mass loss rate ( $\eta=0.8$ ) also provide very similar solutions to the canonical ( $\eta=0.4$ ) case. This indicates that canonical recipes to account for mass loss rate do not al-

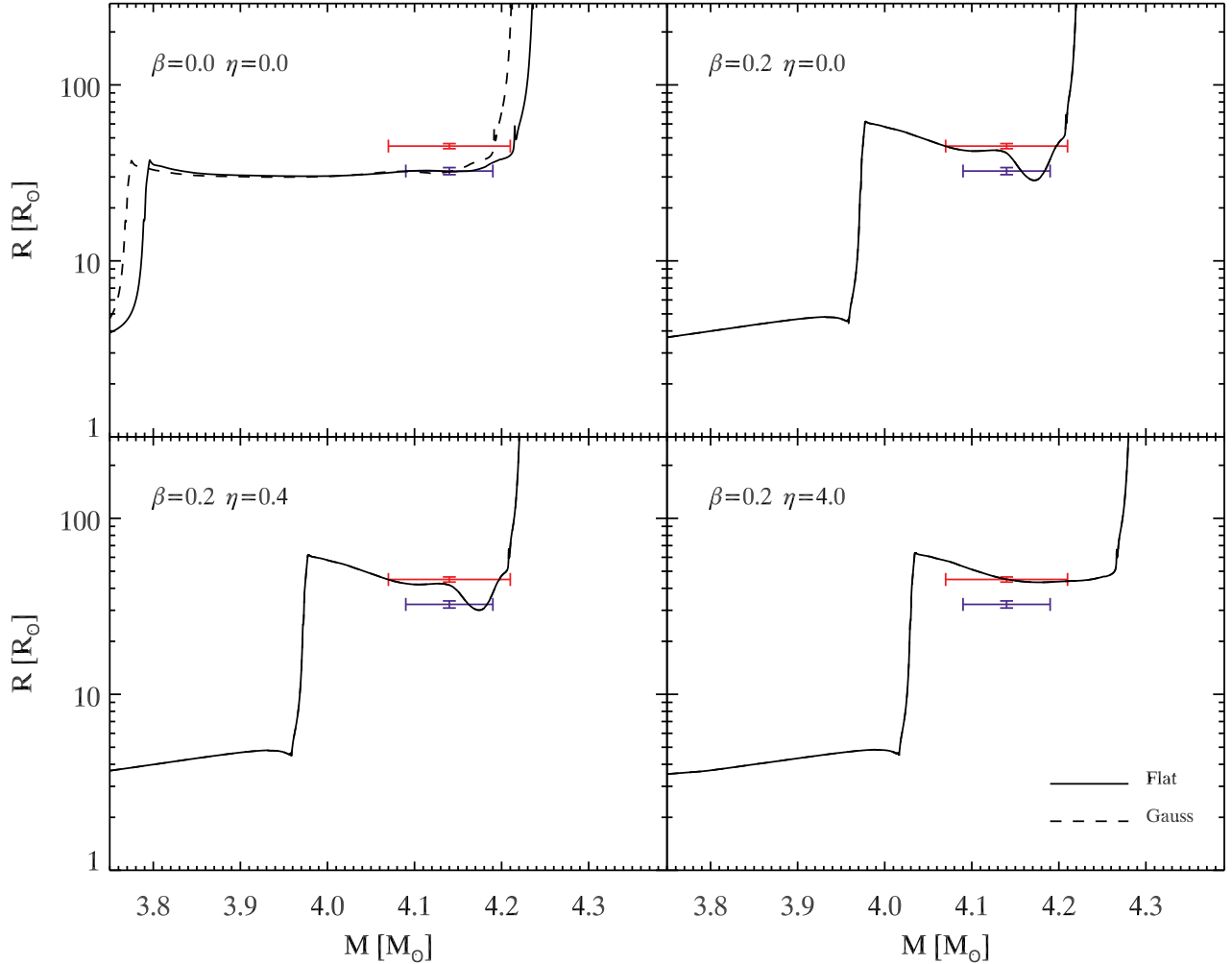


FIG. 4.— Top –Left– Comparison in the stellar mass vs radius plane between the binary components and the isochrone giving the maximum of  $G_C = G_P \times G_S$  (see Table 3). The symbols and the lines are the same as in Fig. 3. Top –Right– Same as top left, but for models accounting for mild ( $\beta=0.2$ ) convective core overshooting. Note that the dashed line overlaps with the solid line, since they attain very similar values in the M–R plane. Bottom – Same as the top right, but for models accounting for a canonical ( $\eta=0.4$ , left) and an enhanced ( $\eta=4.0$ , right) mass loss rate.

low us to provide more quantitative constraints on mass loss efficiency during advanced evolutionary phases (Neilson, Cantiello, & Langer 2011). However, a detailed treatment of the pulsation-driven mass loss inside the instability strip is out of the aim of this investigation.

#### 4.1. Evidence of the most probable solutions

The confidence intervals of the different solutions provide a hint concerning the robustness of individual fits using the different observables. However the precision of the result alone might be a deceptive indicator of the goodness of the fit between theory and data. A narrower confidence interval in the  $(\mu, \tau)$  parameter space does not necessarily imply that the corresponding choice either of the observables, or of the mass prior or of the set of models is better than other possible choices.

A quantitative measurement of the relative goodness of the different solutions can be provided by the Bayes Factor. The Bayes Factor,  $\text{BF}_{ij}$ , between two sets of models is defined as the ratio of the evidence of the two models. The evidence itself is the integral of the Likelihood,

marginalized over the model parameters prior distribution (see, e.g., Bailer-Jones 2011). The evidence gives the total probability of the observed data given the particular set of models considered. Since our sets of models differ for the choice of the mixing length parameter,  $\alpha$ , the core overshooting parameter,  $\beta$ , and the mass-loss parameter,  $\eta$ , we introduce  $\Xi_i = (\alpha_i, \beta_i, \eta_i)$  to identify a particular choice of the three parameters. The evidence is therefore:

$$\mathcal{E}_i(\vec{q}) \equiv \mathcal{E}(\vec{q}|\Xi_i) = \int \mathcal{L}(\tau, \mu, \zeta|\vec{q}, \Xi) f(\tau, \mu, \zeta|\Xi) d\tau d\mu d\zeta \quad (5)$$

The evidence depends on the plane in which the comparison between data and models is performed (L–T, M–R, g–T), on the choice of the prior distribution of the model parameters (i.e.,  $f(\tau, \mu, \zeta|\Xi)$ , in our case flat or Gaussian mass distribution and Gaussian metallicity distribution) and on the  $\Xi$ -set of parameters identifying that set of models (see Fig. 6).  $\mathcal{E}_i(\vec{q})$  is proportional to the total probability of observing the data  $\vec{q}$  under the



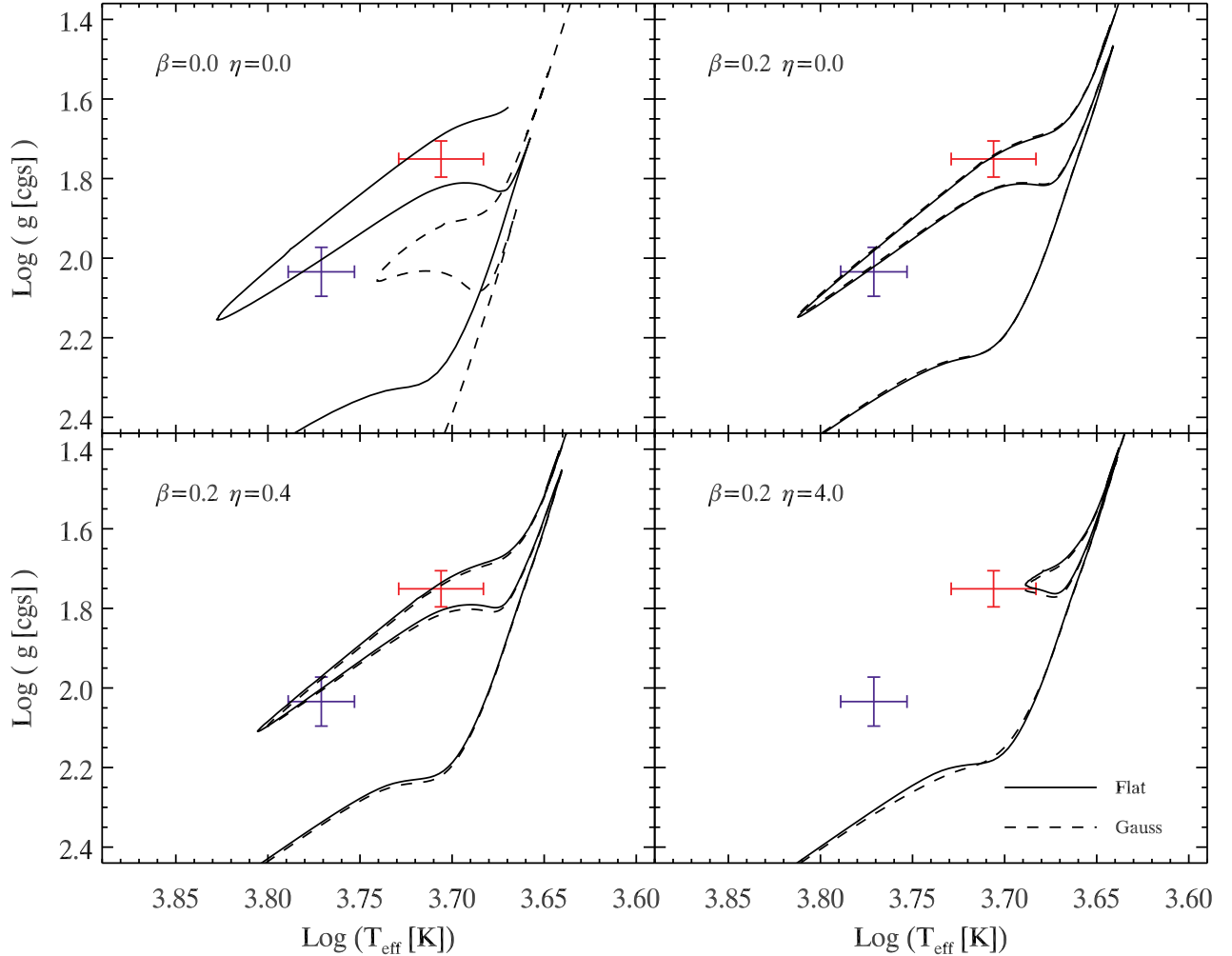


FIG. 5.— Top –Left– Comparison in the logarithmic effective temperature vs logarithmic surface gravity plane between the binary components and the isochrone giving the maximum of  $G_C = G_P \times G_S$  (see Table 3). The symbols and the lines are the same as in Fig. 3. Top –Right– Same as top left, but for models accounting for mild ( $\beta=0.2$ ) convective core overshooting. Bottom – Same as the top right, but for models accounting for a canonical (left,  $\eta=0.4$ ) and an enhanced (right,  $\eta=4.0$ ) mass loss rate.

assumption that the  $\Xi_i$  model is the correct model.

In equation (5) the  $\vec{q}$  observables refer to a single star. The composite evidence for both stars is simply:

$$\mathcal{E}_i(\{\vec{q}_P, \vec{q}_S\}) = \mathcal{E}_i(\vec{q}_P) \times \mathcal{E}_i(\vec{q}_S) \quad (6)$$

From equation (5), it follows that the Bayes factor is:

$$\text{BF}_{ij} = \frac{\mathcal{E}_i}{\mathcal{E}_j} \quad (7)$$

The Bayes factor does not constrain the triplet  $(\tau, \mu, \zeta)$  that provides the highest posterior probability for each set of models. However, it can be used to quantify which set of models, variable plane and prior distribution choice give the best overall agreement with the data. Typically, in order to claim that a set is preferred over another, the Bayes factor should be smaller/larger than one, with either  $\text{BF} < 0.1$  or  $\text{BF} > 10$  (Kass & Raftery 1995).

Table 4 gives the BF values using as a reference the set of models with  $\alpha = 1.74$ ,  $\beta = 0.2$  and  $\eta = 0.4$ , together with the variables  $\vec{q} = (\log g, \log T_{\text{eff}})$  and with the Gaussian mass prior distribution. This reference set gives the

largest evidence for the composite system, therefore it can be considered –within our range of models– the best set of models and the best prior distribution choice to describe the observations. The BFs listed in Table 4 were estimated by dividing the corresponding evidence by the evidence of the reference set either for the primary star (P entries), or for the secondary star (S entries) or for the composite evidence (C entries).

The  $(\beta = 0.2, \eta = 0.0)$  set of models gives BFs for the primary (see Fig. 6), the secondary (see Fig. 7) and the composite system that are very similar to the reference set. Therefore, these two sets give similar likely solutions and with the present data we can not distinguish between them. On the contrary, the set without overshooting,  $\beta = 0$ , and the set with enhanced mass-loss rate,  $\eta = 4.0$ , show very low values of the BFs, suggesting that these parameters can be excluded, hence, confirming the qualitative analysis at the beginning of this section.

It is worth noticing that, the BFs for a given  $\vec{q}$  plane and a given  $\Xi$  set are generally larger when the Gaussian mass prior is used. This suggests that the likelihoods

themselves are already centered in a region of the parameter space which is close to the dynamical mass measurements. Therefore, the Gaussian prior enhances the posterior probabilities when compared with the flat case. This finding is also supported by the fact that several solutions obtained using a flat mass prior distribution are characterized by large confidence intervals (see top panels in Figs. 6 and 7 and the values listed in Table 3). In addition to this, the plane in which the largest BFs are found is the g–T plane. This means that the models, when the measurements of stellar mass, radius and effective temperature are combined, are still able to reproduce these three independent observables, and actually the total probability increases.

Finally, we mention that the presence of two different regions in all the probability diagrams for the secondary component (see Fig. 7) is the consequence of an intrinsic evolutionary feature during the blue loop (helium burning phases). Intermediate-mass stars soon after helium ignition (tip of the red giant branch) move, at fixed stellar mass, towards higher effective temperatures (the so-called blue tip) and then back to lower effective temperatures (Bono et al. 2000, and references therein). During these phases stellar structures with similar masses can be found in similar positions at different ages. However, the contribution of the two probability-regions to the marginal distribution is very different, with the main region contributing a much larger probability than the secondary one. The latter region only causes an increase in the skewness of the marginal distributions, without manifestation of secondary maxima.

## 5. THE COLOR-MAGNITUDE DIAGRAM

The binary system CEP0227 offers a unique opportunity to test the plausibility of the physical assumptions adopted in evolutionary and pulsation models because the comparison between theory and observations can be performed by using observables (luminosity, radius, effective temperature, surface gravity) directly predicted by evolutionary models. This means that these observables do not need to be transformed into the observational plane. However, the Cepheid mass discrepancy problem arises from the comparison between evolutionary prescriptions and observations in the CMD. The main advantage in using this plane to estimate the evolutionary mass is that the estimate only relies on two mean magnitudes in different photometric bands. The main drawback is that the mass estimates are affected by uncertainties in the true distance modulus and in the reddening. To overcome the latter problem the mass estimates have also been performed in CMDs based on NIR bands (Bono et al. 2001).

Absolute distance determination and NIR magnitudes for the binary CEP0227 are not available yet. We have already collected new NIR time series data and we plan to provide a detailed analysis of the CMD and of the color-color plane in a forthcoming investigations.

However, the solutions based on theoretical observables do allow us to constrain the possible occurrence of thorny systematic uncertainties in the bolometric corrections and in the color-temperature relations adopted to transform theoretical predictions into the observational plane. Moreover, we can also estimate the reddening of the system by assuming as a prior a Gaussian distribution on the

true distance modulus. We used the theoretical solution which gives the largest evidence for the composite system, i.e. the 151 Myr isochrone for the  $\beta = 0.2, \eta = 0.4$  set. This is the most probable age for the composite  $G(\tau)$  in the case of the g–T plane. We transformed the isochrone into the Johnson–Kron–Cousins photometric system using the spectra provided by Castelli & Kurucz (2003) based on the ATLAS9 model atmospheres (see Fig. 8). We also performed a test by using the spectra based on the atmosphere models provided by the PHOENIX code in the version by Brott & Hauschildt (2005). We found that the difference—in the typical temperature, metallicity and surface gravity regime of the binary we are dealing with—is negligible, therefore in the following we adopt the evolutionary models transformed using the ATLAS9 models.

The comparison into the observational plane (CMD) between the isochrone of the most probable solution and observations provides independent estimates of both the reddening and the true distance modulus of the binary system. The reddening in the V,I-bands was fixed by adopting the Cardelli et al. (1989) extinction law. The solution was found by maximizing the probability:

$$p(E(B-V), DM) = \prod_{i=P,S} \frac{1}{2\pi\sigma_{V_i}\sigma_{(V-I)_i}} \times \int \exp \left[ -\frac{\chi_{V_i}^2 + \chi_{(V-I)_i}^2}{2} - \frac{(DM - DM_0)^2}{2\sigma_{DM_0}^2} \right] dm \quad (8)$$

where:

$$\chi_{V,i} = \frac{V_i - V(m; E(B-V), DM)}{\sigma_{V_i}}$$

and

$$\chi_{(V-I)_i} = \frac{(V-I)_i - (V-I)(m; E(B-V), DM)}{\sigma_{(V-I)_i}}$$

The index  $i$  runs on the primary and on the secondary star ( $P, S$ ),  $V_i$  and  $(V-I)_i$  are the observed mean magnitudes and colors with their errors  $\sigma_{V_i}$  and  $\sigma_{(V-I)_i}$ . The theoretical quantities are function of the mass along the isochrone and of the adopted distance modulus and reddening. The integral is performed along the isochrone integrating over the mass of the models. Given the available information on the LMC distance modulus, we used a Gaussian prior with mean and standard deviations given by  $\mu = 18.45 \pm 0.04$  mag (Storm et al. 2011).

Fig. 8 shows the 151 Myr isochrone in the V, V-I CMD, with a reddening of  $0.142_{-0.010}^{+0.005}$  mag and a distance of  $18.53_{-0.02}^{+0.02}$  mag as found by maximizing equation (8). This estimate of the reddening agrees very well with the reddening estimates based on Schlegel’s map, namely  $0.15 \pm 0.03$  mag (Schlegel, Finkbeiner, & Davis 1998). The same outcome applies to the LMC distance, since it agrees with similar estimates available in the literature (Storm et al. 2011, and references therein). This evidence is also supported by the fact that the plane of the LMC is also tilted along the line of sight and we are not applying any correction for the position of the binary system (Persson et al. 2004). In order to constrain the sensitivity of both distance modulus and red-

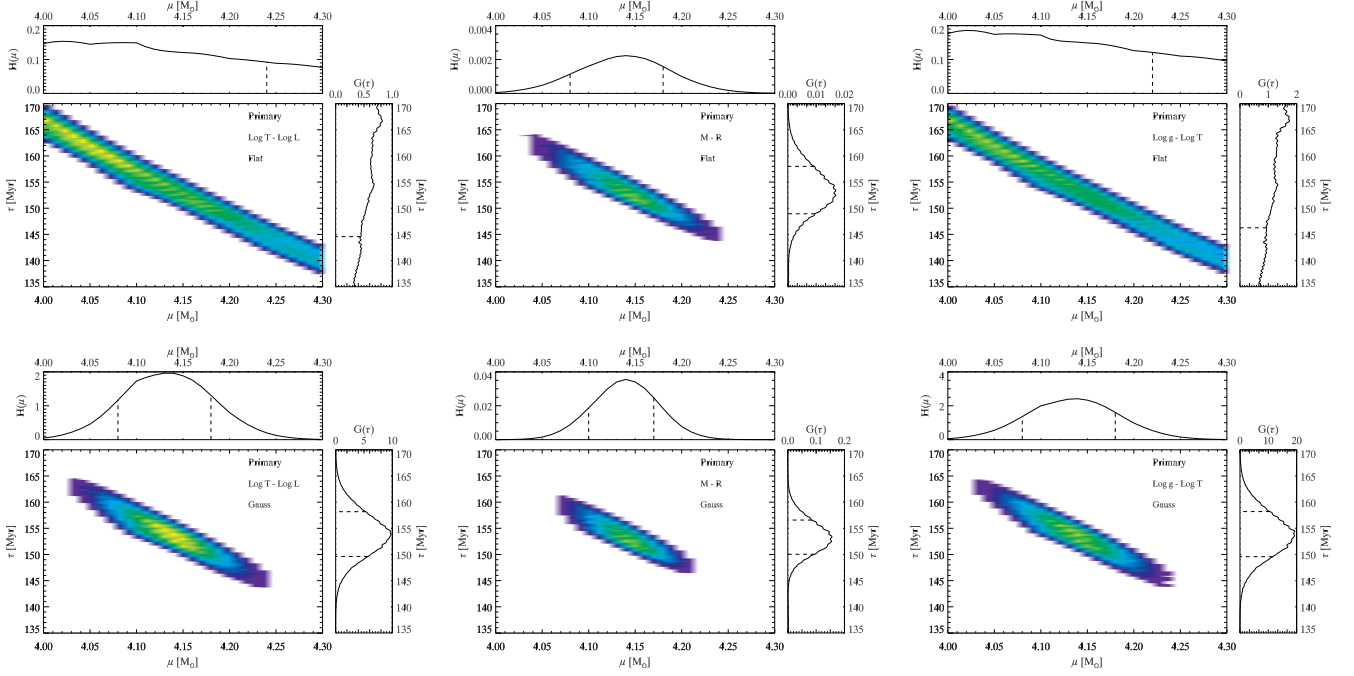


FIG. 6.— Posterior probability distributions for the primary component according to the set of evolutionary models constructed by assuming  $\beta = 0.2, \eta = 0.4$  in the L–T (left), in the M–R (middle) and in the g–T (right) plane using either a flat (top panels) or a Gaussian (bottom panels) prior on the mass distribution. Each 2D probability is obtained after marginalizing over the metallicity Gaussian distribution for LMC Cepheids. In each panel the probability was normalized to its maximum value for displaying purposes, therefore the color coding range from 0 (blue) to 1 (red) normalized probability. The top and the right insets display the marginalization for the stellar age and the stellar mass of the primary, respectively. The vertical dashed lines show the confidence intervals. The y-axis of the insets show the actual value of the marginal distributions before the normalization.

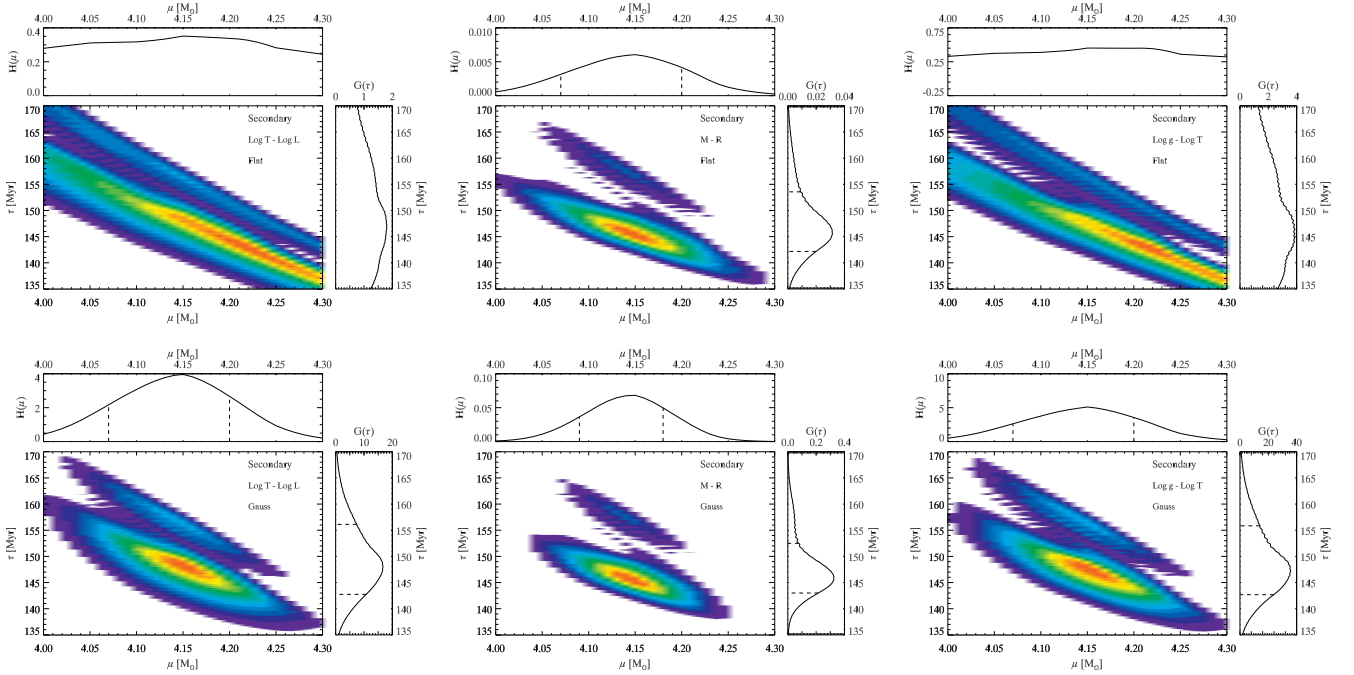


FIG. 7.— Same as Fig. 6, but for the secondary component.

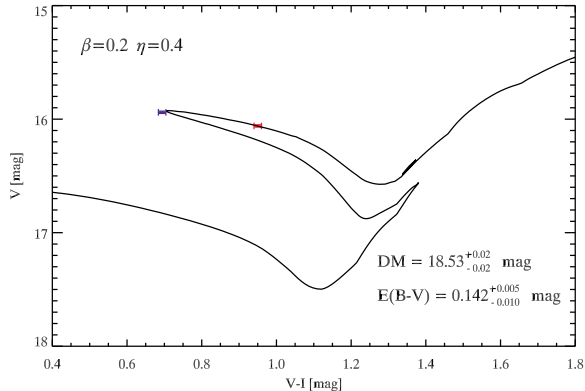


FIG. 8.— The isochrone of the most probable solution ( $\beta=0.2$ ,  $\eta=0.4$ ,  $g$ - $T$  plane, Gaussian mass prior) transformed into the  $V, V-I$  color-magnitude diagram. The blue and the red symbols display the Primary (Cepheid) and the Secondary component of the binary system. The true distance modulus and the reddening estimated using the combined system are also labeled.

dening on the prior we also adopted a flat prior between  $\mu=18$  and 19 mag. Note that the adopted interval is significantly larger than the range of LMC distances indicated in literature and we found a true distance modulus of  $\mu=18.57^{+0.13}_{-0.01}$  mag and a reddening of  $E(B-V) = 0.1275^{+0.0025}_{-0.07}$  mag. The new estimates have larger confidence intervals, but they agree quite well with the estimates based on the Gaussian prior. The above findings and the robustness of the most probable solution (see Fig. 9) provide an independent support to the current set of atmosphere models adopted to transform theory into the observational plane (Castelli & Kurucz 2003).

## 6. SUMMARY AND FINAL REMARKS

The discovery by OGLEIII of eclipsing binary systems in the Large Magellanic Cloud hosting classical Cepheids provided the unique opportunity of measure their masses with a precision ranging from 1% (CEP0227) to 1.5% (CEP1812, paper II). It goes without saying that the new measurements will allow us to constrain the precision and the plausibility of the the input physics and physical assumptions adopted in constructing both evolutionary and pulsation models. In this investigation, we addressed the evolutionary mass and the age of the binary system CEP0227. We adapted the general Bayesian approach developed by Gennaro, Prada Moroni, & Tognelli (2012) to constrain the physical parameters of the binary components.

In order to provide robust statistical solutions, we computed several sets of evolutionary models by covering a broad range of chemical compositions (see Table 1) and stellar masses. To constrain the dependence on the free parameters currently adopted in canonical evolutionary models, independent sets of models were constructed by assuming two different values of the mixing length parameter ( $\alpha=1.74, 1.90$ ). Moreover, to account for the possible occurrence of extra-mixing during central hydrogen burning phases, the models were constructed either by neglecting or by including a moderate convective core overshooting ( $\beta_{ov}=0.2$ ). Finally, to account for the mass loss during evolved evolutionary phases the models were constructed either by neglecting or by including

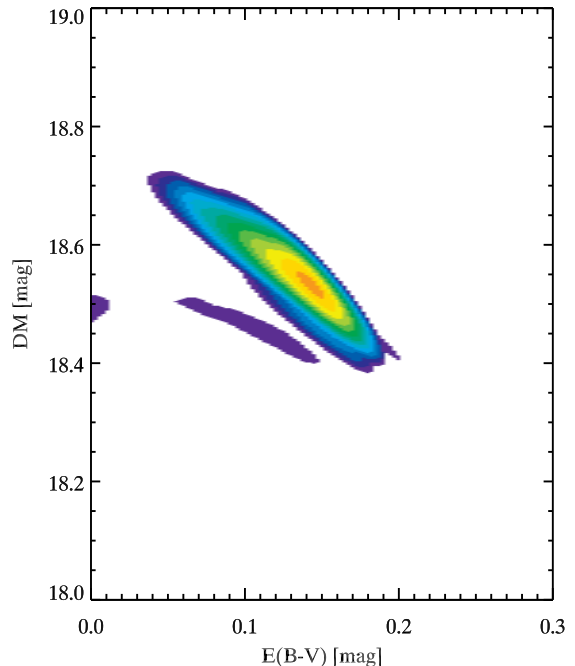


FIG. 9.— Robustness of the most probable solutions for the true distance modulus and the reddening of the binary system obtained using the isochrone with the largest evidence and a prior on the true distance modulus ( $18.45 \pm 0.04$  mag). The color coding shows the transition from less (blue) to more (red) accurate most probable solutions.

mass loss. To mimic different efficiencies in the mass loss rate, we constructed sets of models accounting either for canonical ( $\eta=0.4, 0.8$ ) or for enhanced ( $\eta=4$ ) mass loss rates (see Table 1).

To overcome possible deceptive errors in the estimate of the physical parameters, the comparison between theory and observations was performed in three different planes: luminosity vs effective temperature ( $\log L, \log T_{eff}$ ), mass vs radius (M,R) and surface gravity vs effective temperature ( $\log g, \log T_{eff}$ ). We computed an independent solution (mass, age, chemical composition) in the three quoted planes for every set of evolutionary models we have constructed. Note that individual solutions were computed by adopting two different priors for the stellar mass. We adopted either a flat distribution over the entire range of stellar masses covered by computations or a Gaussian distribution anchored to the mean and the standard deviation of the dynamical mass measurements (paper I). We also adopted a Gaussian prior for the metallicity, in particular we adopted the mean and the standard deviation for LMC Cepheids recently provided by Romaniello et al. (2008) by using high-resolution, high signal to noise spectra.

The main results we obtained in the comparison between theory and observations are the following:

- The most probable solutions are minimally affected by the adopted mixing length parameter, within the range covered by our models.
- The most probable solutions based on a Gaussian mass prior are typically more accurate than those based on the flat mass prior.

- The most stringent test to constrain the models were obtained in the  $g$ - $T$  plane, due to the fact that the adopted parameters involve three independent observables, namely mass, radius and temperature. In this plane, the most probable solutions were obtained by using the evolutionary models that account for a moderate convective overshooting ( $\beta_{ov}=0.2$ ) and canonical mass loss rate ( $\eta=0.4$ ). In particular, we found that the mass of the primary (Cepheid) is  $M=4.14^{+0.04}_{-0.05} M_{\odot}$ , while for the secondary is  $M=4.15^{+0.04}_{-0.05} M_{\odot}$ . Note that current estimates do agree at the 1% level with dynamical measurements. We found ages for the individual components and for the combined system ( $t=151_3^{+4}$  Myr) do agree at the 5% level, supporting once again the robustness of the solution. It is noteworthy that similar solutions are obtained by using moderate convective overshooting ( $\beta_{ov}=0.2$ ) and no mass loss ( $\eta=0$ ). This indicates that either a vanishing or a canonical mass loss rate play a marginal role in the Cepheid mass discrepancy. Current findings support the preliminary results concerning the evolutionary mass of CEP0227 provided by Cassisi & Salaris (2011). They also suggest that evolutionary masses based on evolutionary models accounting for moderate convective core overshooting – a typical assumption in the comparison between theory and observations (Pietrinferni et al. 2006) – agree quite well with the dynamical mass of Cep0227. The overall agreement among dynamical, evolutionary and pulsation masses will be addressed in a forthcoming paper in which we plan to constrain the pulsation mass using independent observables.
- The most probable solutions based on the models constructed by assuming a moderate convective overshooting ( $\beta_{ov}=0.2$ ) and an enhanced mass loss rate ( $\eta=4$ ) present large confidence interval when compared with the solutions based on canonical mass loss rate (see Table 3). Note that current finding should be cautiously treated. The reason is twofold. The difference between the estimated masses and the dynamical masses, taken at face value, do agree at the 1% level. We are assuming a very crude approximation to account for the mass loss, while current empirical and theoretical findings indicate that the mass loss might be driven by the pulsation instability (Neilson, Cantiello, & Langer 2011; Matthews et al. 2011). This hypothesis is further supported by the recent results obtained by Neilson et al. (2011). They found that the observed period change of Polaris implies a mass loss rate of  $\approx 10^{-6} M_{\odot} \text{ yr}^{-1}$ , and in turn a new firm empirical argument for enhanced mass loss in Cepheids.

The above discussion concerning the formal precision of the results relies on the width of the confidence interval. However, a solution characterized by a narrow confidence interval might not be the most probable solution. The Bayes Factor between two sets of models

is a more robust statistical parameter to constrain on a quantitative basis the most probable solutions.

By using the Bayes Factor the main results we obtained in the comparison between theory and observations are the following:

- The solutions with the largest evidence were obtained in the  $g$ - $T$  plane by using sets of models that account for a moderate convective core overshooting ( $\beta_{ov}=0.2$ ) and either a vanishing ( $\eta=0$ ) or a canonical mass loss rate ( $\eta=0.4$ ) give very similar results. This finding supports the results based on the confidence interval.
- The solutions based on sets of models that either neglect convective core overshooting or account for an enhanced mass loss rate ( $\eta=4$ ) are characterized by very low Bayes Factors. Thus suggesting that these two sets of models give a poorer description of the observed properties of the binary system.

We also transformed the isochrone of the most probable solution ( $\beta=0.2$ ,  $\eta=0.4$ ,  $g$ - $T$  plane, Gaussian mass prior) mentioned above into the observational plane using the atmosphere models provided by Castelli & Kurucz (2003). By assuming a Gaussian metallicity prior distribution for the Cepheid metallicity and by assuming the Cardelli et al. (1989) reddening law, we found a true distance modulus  $-18.53^{+0.02}_{-0.02}$  mag– and a reddening value  $-E(B-V)=0.142^{+0.005}_{-0.010}$  mag– that agree quite well with similar estimates available in the literature (Schlegel, Finkbeiner, & Davis 1998; Persson et al. 2004; Storm et al. 2011). The use of a flat prior on the LMC distance, minimally affects these results. A more detailed discussion concerning new independent distances of the binary system and of the Cepheid will be addressed in a forthcoming investigation.

Intrinsic variables in eclipsing binary systems are a fundamental laboratory to constrain the input physics of both evolutionary and pulsation models. This was considered till a few years ago a broken ground for quantitative astrophysics, due to the limited number of known systems and the lack of homogeneous and precise photometric and spectroscopic data. The unprecedented photometric catalogs released by microlensing experiments (EROS, OGLEIII) together with currently underway optical (PanSTARRS-1, Stubbs et al. (2010); Palomar Transient Factory, van Eyken et al. (2011); CHASE, Foerster, et al. (2010)) and NIR (VVV, Minniti et al. (2010)) surveys and the spectrographs available at 8m class telescopes, are a very good viaticum in waiting for GAIA.

It is a pleasure to thank F. Caputo for many useful discussions concerning evolutionary and pulsation properties of classical Cepheids and M. Dell’Omodarme for his invaluable help in computer programming. We also acknowledge an anonymous referee for his/her positive opinion concerning the content of the paper and for his/her sharp and pertinent comments that helped us to improve the content and the readability of the manuscript. We gratefully acknowledge financial support for this work from the Chilean Center for Astrophysics FONDAF 15010003 and the BASAL Centro de

Astrofísica y Tecnologías Afines (CATA) PFB-06/2007. Support from the Polish grants N203 387337, the IDEAS Plus, the FOCUS and the TEAM subsidies of the Fundation for Polish Science (FNP) are also acknowledged.

During the preparation of this paper M. Gennaro has been a member and would like to acknowledge the "International Max Planck Research School for Astronomy and Cosmic Physics" at the University of Heidelberg, IMPRS-HD, Germany.

## REFERENCES

- Alcock, C. et al. 1999, *AJ*, 117, 920  
 Angulo C., Arnould, M., Rayet, M., et al. 1999, *Nuclear Physics A*, 656, 3  
 Asplund, M.; Grevesse, N.; Sauval, A. J.; & Scott, P. 2009, *ARA&A*, 47, 481  
 Badnell, N. R. et al. 2005, *MNRAS*, 360, 458  
 Bailer-Jones, C. A. L. 2011, *MNRAS*, 416, 1163  
 Barmby, P.; Marengo, M.; Evans, N. R.; Bono, G.; Huelsman, D.; Su, K. Y. L.; Welch, D. L.; & Fazio, G. G. 2011, *AJ*, 141, 42  
 Barmina, R.; Girardi, L.; Chiosi, C. 2002, *A&A*, 385, 847  
 Beaulieu, J. P., Buchler, J. R., Kollath, Z. 2001, *A&A*, 373, 164  
 Becker, S. A., & Iben, I., Jr. 1979, *ApJ*, 232, 831  
 Becker, S. A.; Iben, I., Jr.; Tuggle, R. S. 1977, *ApJ*, 218, 633  
 Bemmerer, D., Confortola, F., Lemut, A., et al. 2006, *Nuclear Physics A* 779, 297  
 Bertelli, G.; Nasi, E.; Girardi, L.; Marigo, P. 2009, *A&A*, 508, 355  
 Böhm-Vitense, E. 1958, *Zs.f.Ap.*, 46, 108  
 Bonanos, A. Z. et al. 2009, *AJ*, 138, 1003  
 Bonanos, A. Z. et al. 2010, *AJ*, 140, 416  
 Bono, G., Caputo, F., Cassisi, S., Marconi, M., Piersanti, L., & Tornambe, A. 2000, *ApJ*, 543, 955  
 Bono, G. Gieren, W. P., Marconi, M., Fouqué, P., & Caputo, F. 2001, *ApJ*, 563, 319  
 Bono, G. et al. 2002, *ApJ*, 565, L83  
 Brocato, E. & Castellani, V. 1993, *ApJ*, 410, 99  
 Brocato, E.; Castellani, V.; Di Carlo, E.; Raimondo, G.; & Walker, A. R. 2003, *AJ*, 125, 3111  
 Brott, I.; & Hauschildt, P. H. 2005, in *ESA Special Publication, Vol. 576, The Three-Dimensional Universe with Gaia*, ed. C. Turon, K. S. O'Flaherty, & M. A. C. Perryman, 565  
 Brott, I. et al. 2011a, *A&A*, 530, 115  
 Brott, I. et al. 2011b, *A&A*, 530, 116  
 Caputo, F. et al. 2005, *ApJ*, 629, 1021  
 Cardelli, J. A., Clayton, G. C., & Mathis, J. S. 1989, *ApJ*, 345, 245  
 Cassisi, S. 2004, in *IAU Colloq. 193, Variable Stars in the Local Group*, ed. D.W. Kurtz & K.R. Pollard (San Francisco: ASP), 489  
 Cassisi, S., & Salaris, M. 2011, *ApJ*, 728, L43  
 Castellani, V., Chieffi, A. & Straniero, O. 1990, *ApJS*, 74, 463  
 Castellani, V., Degl'Innocenti, S., Girardi, L., Marconi, M., Prada Moroni, P. G., & Weiss, A. 2000, *A&A*, 354, 150  
 Castellani, V., Giannone, P., & Renzini, A. 1971a, *Ap&SS*, 10, 340  
 Castellani, V., Giannone, P., & Renzini, A. 1971b, *Ap&SS*, 10, 355  
 Castelli, F., & Kurucz, R. L. 2003, *Modelling of Stellar Atmospheres*, 210, 20P  
 Charbonnel, C. & Lagarde, N. 2010, *A&A*, 522, 10  
 Chiosi, C., & Maeder, A. 1986, *ARA&A*, 24, 329  
 Christy, R. F. 1966, *ApJ*, 145, 340  
 Christy, R. F. 1970, *JRASC*, 64, 8  
 Cordier, D. et al. 2002, *A&A*, 392, 169  
 Cyburt, R. H., Fields, B. D., Olive, K. A., & Skillman, E. 2005, *Aph*, 23, 313  
 Deasy, H. P. 1988, *MNRAS*, 231, 673  
 Degl'Innocenti, S., Prada Moroni, P. G., Marconi, M., & Ruoppo, A. 2008, *Ap&SS*, 316, 25  
 Dell'Omodarme, E., Valle, G., degl'Innocenti, S., Prada Moroni, P. G. 2011, *A&A*, submitted  
 Efremova, B. V. et al. 2011, *ApJ*, 730, 88  
 Evans, N. et al. 2005a, *AJ*, 130, 789  
 Ferguson, J.W., Alexander, D.R., Allard, F., et al. 2005, *ApJ*, 623, 585  
 Flynn, C. 2004, *PASA*, 21, 126  
 Fricke, K., Stobie, R. S., & Strittmatter, P. A. 1971, *MNRAS*, 154, 23  
 Foerster, F., López, N., Maza, J., Kubánek, P., Pignata, G. 2010, *AdAst*, 107569  
 Gennaro, M., Prada Moroni, P. G., Degl'Innocenti, S. 2010, *A&A*, 518, 13  
 Gennaro, M., Prada Moroni, P. G., & Tognelli, E. 2011, *MNRAS*, 420, 986  
 Hammer, J.W., Fey, M., Kunz, R. et al. 2005, *Nuclear Physics A*, 758, 363  
 Hofmeister, E., Kippenhahn, R., & Weigert, A. 1964, *ZA*, 60, 57  
 Hunter I. et al. 2009a, *A&A*, 496, 841  
 Hunter I. et al. 2009b, *A&A*, 504, 211  
 Iglesias, C. A., Rogers, F. J. 1991, *ApJ*, 371, 408  
 Iglesias, C., & Rogers, F.J. 1996, *ApJ*, 464, 943  
 Imbriani, G., Costantini, H., Formicola, A., et al. 2005, *Eur. Phys. J. A*, 25, 455  
 Jimenez, R., Flynn, C., MacDonald, J., & Gibson, B. K. 2003, *Science*, 299, 1552  
 Jorgensen, B. R., & Lindegren, L. 2005, *A&A*, 436, 127  
 Kass, R. & Raftery, A. 1995, *Journal of the American Statistical Association*, 90, 773  
 Karakas, A. I., Lattanzio, J. C. 2003, *PASA*, 20, 279  
 Keller, S. C., Wood, P. R. 2002, *ApJ*, 578, 144  
 Keller, S. C., Wood, P. R. 2006, *ApJ*, 642, 834  
 Keller, S. C., 2008, *ApJ*, 677, 483  
 Kervella, P., Merand, A., & Gallenne, A. 2009, *A&A*, 498, 425  
 Kervella, P.; Merand, A.; Perrin, G.; Coud du Foresto, V. 2006, *A&A*, 448, 623  
 Kervella, P., Merand, A., Szabados, L., Fouqué, P., Bersier, D., Pompei, E., Perrin, G. 2008, *A&A*, 480, 167  
 Komatsu, E. et al. 2011, *ApJS*, 192, 18  
 Korn, A. J.; Nieva, M. F.; Dafon, S.; Cunha, K. 2005, *ApJ*, 633, 899  
 Langer, N. 1991, *A&A*, 252, 669  
 Lemut, A., Bemmerer, D., Confortola, F. et al. 2006, *Phys. Lett. B*, 634, 483  
 Maeder, A. & Meynet, G. 2000, *ARA&A*, 38, 143  
 Marengo, M. et al. 2010b, *ApJ*, 725, 2392  
 Marengo, M.; Evans, N. R.; Barmby, P.; Bono, G.; Welch, D. L.; Romaniello, M. 2010a, *ApJ*, 709, 120  
 Matthews, L. D., Marengo, M., Evans, N. R., & Bono, G. *ApJ*, in press, arXiv1112.0028  
 McAlary, C. W., & Welch, D. L. 1986, *AJ*, 91, 1209  
 Merand, A. et al. 2006, *A&A*, 453, 155  
 Merand, A. et al. 2007, *ApJ*, 664, 1093  
 Meynet, G., & Maeder, A. 2002, *A&A*, 390, 561  
 Minniti, D., et al. 2010, *NewA*, 15, 433  
 Moskalik, P., Buchler, J. R., Marom, A. 1992, *ApJ*, 385, 685  
 Neilson, H. R., & Lester, J. B. 2008, *ApJ*, 684, 569  
 Neilson, H. R., Ngeow, C.-C., Kanbur, S. M., & Lester, J. B. 2009, *ApJ*, 692, 81  
 Neilson, H. R., Cantiello, M., & Langer, N. 2011, *A&A*, 529, L9  
 Neilson, H. R., Engle, S. G., Guinan, E., Langer, N., Wasatonic, R. P., & Williams, D. B. 2012, *ApJ*, 745, L32  
 Nieuwenhuijzen, H. & de Jager, C. 1990, *A&A*, 231, 134  
 Pagel, B. E. J., & Portinari, L. 1998, *MNRAS*, 298, 747  
 Persson, S. E., Madore, B. F., Krzeminski, W., Freedman, W. L., Roth, M., Murphy, D. C. 2004, *AJ*, 128, 2239  
 Peimbert, M., Luridiana, V., & Peimbert, A. 2007, *ApJ*, 666, 636  
 Pietrinferni, A., Cassisi, S., Salaris, M., Castelli, F. 2004, *ApJ*, 612, 168  
 Pietrinferni, A., Cassisi, S., Salaris, M., Castelli, F. 2006, *ApJ*, 642, 797  
 Pietrzynski, G. et al. 2010, *Nature*, 468, 542, paper I  
 Pietrzynski, G. et al. 2011, *ApJ*, 742, L20, paper II  
 Pompeia, L., et al. 2008, *A&A*, 480, 379  
 Potekhin, A.Y. 1999, *A&A*, 351, 787  
 Reimers, D. 1975, *Memories de la Societe Royal des Sciences de Liege*, 8, 369  
 Rogers, F.J., Swenson, F.J., & Iglesias, C.A. 1996, *ApJ*, 456, 902  
 Romaniello, M. et al. 2008, *A&A*, 488, 731  
 Seaton, M. J., et al. 1994, *MNRAS*, 266, 805  
 Sanna et al. 2009, *ApJ*, 699, L84  
 Schlegel, D. J., Finkbeiner, D. P., Davis, M. 1998, *ApJ*, 500, 525  
 Schroeder, K.-P., Cuntz, M. 2005, *ApJ*, 630, L73  
 Shternin, P.S. & Yakovlev, D.G. 2006, *PhRvD*, 74(4), 3004  
 Steigman, G. 2006, *IJMPE*, 15, 1  
 Stobie, R. S. 1969, 144, 485  
 Storm, J., Gieren, W., Fouqué, P., Barnes, T. G., Soszyński, I., Pietrzyński, G., Nardetto, N., Queloz, D. 2011, *A&A*, 534, A95  
 Stothers, R., & Chin, C.-W. 1978, *ApJ*, 226, 231  
 Stothers, R. B. & Chin, C.-W. 1993, *ApJ*, 412, 294  
 Stothers, R. B. & Chin, C.-W. 1996, *ApJ*, 469, 166  
 Stubbs, C. W. et al. 2010, *ApJS*, 191, 376  
 Testa, V. et al. 1999, *AJ*, 118, 2839  
 Tognelli, E., Prada Moroni, P. G., & Degl'Innocenti, S. 2011, *A&A*, 533, 109

TABLE 1  
INTRINSIC STELLAR PARAMETERS ADOPTED TO COMPUTE EVOLUTIONARY TRACKS.

$Z^a$	$Y^a$	$\alpha_{ml}^b$	$\beta_{ov}^c$	$\eta^d$				
0.004	0.256	1.74	0.0	0	0.4	0.8	4.0	
0.005	0.258	1.74	0.0	0	0.4	0.8	4.0	
0.006	0.260	1.74	0.0	0	0.4	0.8	4.0	
0.007	0.262	1.74	0.0	0	0.4	0.8	4.0	
0.008	0.265	1.74	0.0	0	0.4	0.8	4.0	
0.004	0.256	1.90	0.0	0	0.4	0.8	4.0	
0.005	0.258	1.90	0.0	0	0.4	0.8	4.0	
0.006	0.260	1.90	0.0	0	0.4	0.8	4.0	
0.007	0.262	1.90	0.0	0	0.4	0.8	4.0	
0.008	0.265	1.90	0.0	0	0.4	0.8	4.0	
0.004	0.256	1.74	0.2	0	0.4	0.8	4.0	
0.005	0.258	1.74	0.2	0	0.4	0.8	4.0	
0.006	0.260	1.74	0.2	0	0.4	0.8	4.0	
0.007	0.262	1.74	0.2	0	0.4	0.8	4.0	
0.008	0.265	1.74	0.2	0	0.4	0.8	4.0	
0.004	0.256	1.90	0.2	0	0.4	0.8	4.0	
0.005	0.258	1.90	0.2	0	0.4	0.8	4.0	
0.006	0.260	1.90	0.2	0	0.4	0.8	4.0	
0.007	0.262	1.90	0.2	0	0.4	0.8	4.0	
0.008	0.265	1.90	0.2	0	0.4	0.8	4.0	

<sup>a</sup> Metal ( $Z$ ) and helium ( $Y$ ) abundance by mass.

<sup>b</sup> Mixing length parameter.

<sup>c</sup> Overshooting parameter.

<sup>d</sup> Mass loss parameter.

TABLE 2  
ADOPTED INTRINSIC PARAMETERS FOR THE BINARY SYSTEM CEP0227.

Parameter	Value	Ref. <sup>a</sup>
Mass ( $M/M_{\odot}$ ) <sup>b</sup>	4.14±0.05	1
...	4.14±0.07	1
Radius ( $R/R_{\odot}$ ) <sup>b</sup>	32.4±1.5	1
...	44.9±1.5	1
$T_{eff}$ (K) <sup>b</sup>	5,900±250	1
...	5,080±270	1
$V$ (mag) <sup>b,c</sup>	15.940±0.001	
...	16.06±0.02	
$I$ (mag) <sup>b,c</sup>	15.246±0.001	
...	15.11±0.01	
$\mu$ (mag) <sup>d</sup>	18.45±0.04	2
$E(B - V)$ (mag) <sup>e</sup>	0.15±0.03	3
[Fe/H] (dex) <sup>f</sup>	-0.33±0.05	4

<sup>a</sup> References: 1) Pietrzynski et al. (2010); 2) Storm et al. (2011); 3) Schlegel et al. (1998); 4) Romaniello et al. (2008).

<sup>b</sup> The first line, for each parameter, refers to the primary (Cepheid), while the second one to the secondary (companion).

<sup>c</sup> Apparent  $V$  and  $I$ -band magnitudes. The mean magnitude of the Cepheid was estimated in flux and then transformed into magnitude.

<sup>d</sup> True distance modulus.

<sup>e</sup> Reddening according to the Schlegel's map.

<sup>f</sup> Mean iron abundance (scaled-solar mixture).

Valle, G.; Marconi, M.; Degl'Innocenti, S.; Prada Moroni, P. G.  
2009, *A&A*, 507, 1541

Venn, K. A. 1999, *ApJ*, 518, 405

van Eyken, J. C. 2011, *AJ*, 142, 60

TABLE 3  
 MOST PROBABLE AGES AND MASSES FOR THE DIFFERENT OBSERVABLES, THE DIFFERENT SETS OF EVOLUTIONARY MODELS AND FOR THE PRIORS ADOPTED FOR THE STELLAR MASS DISTRIBUTION.

MP <sup>a</sup>	Obs. <sup>b</sup>	Star <sup>c</sup>	$\beta = 0.0, \eta = 0$		$\beta = 0.2, \eta = 0$		$\beta = 0.2, \eta = 0.4$		$\beta = 0.2, \eta = 4.0$		
			Age <sup>d</sup> [Myr]	Mass <sup>d</sup> [ $M_{\odot}$ ]	Age <sup>e</sup> [Myr]	Mass <sup>e</sup> [ $M_{\odot}$ ]	Age <sup>f</sup> [Myr]	Mass <sup>f</sup> [ $M_{\odot}$ ]	Age <sup>g</sup> [Myr]	Mass <sup>g</sup> [ $M_{\odot}$ ]	
Flat	L-T	P	115 <sup>+44</sup> <sub>-9</sub>	4.50 <sup>+0.18</sup> <sub>-0.52</sub>	165 <sup>+32</sup> <sub>-19</sub>	3.98 <sup>+0.24</sup> <sub>-0.29</sub>	167 <sup>+29</sup> <sub>-22</sub>	3.97 <sup>+0.27</sup> <sub>-0.27</sub>	137 <sup>+95</sup> <sub>-42h</sub>	3.60 <sup>+1.05</sup> <sub>-0.15</sub>	
		S	96 <sup>+20</sup> <sub>-6</sub>	4.70 <sup>+0.16</sup> <sub>-0.28</sub>	143 <sup>+36</sup> <sub>-11</sub>	4.15 <sup>+0.19</sup> <sub>-0.33</sub>	147 <sup>+30</sup> <sub>-15</sub>	4.15 <sup>+0.20</sup> <sub>-0.32</sub>	148 <sup>+26</sup> <sub>-12</sub>	4.19 <sup>+0.14</sup> <sub>-0.33</sub>	
		C	107 <sup>+12</sup> <sub>-10</sub>		154 <sup>+21</sup> <sub>-13</sub>		150 <sup>+24</sup> <sub>-9</sub>		137 <sup>+67</sup> <sub>-9h</sub>		
	M-R	P	134 <sup>+11</sup> <sub>-6</sub>	4.13 <sup>+0.04</sup> <sub>-0.05</sub>	154 <sup>+4</sup> <sub>-5</sub>	4.10 <sup>+0.07</sup> <sub>-0.02</sub>	153 <sup>+5</sup> <sub>-4</sub>	4.14 <sup>+0.04</sup> <sub>-0.05</sub>	145 <sup>+21</sup> <sub>-11h</sub>	4.14 <sup>+0.05</sup> <sub>-0.07</sub>	
		S	114 <sup>+30</sup> <sub>-4</sub>	4.19 <sup>+0.05</sup> <sub>-0.09</sub>	145 <sup>+7</sup> <sub>-3</sub>	4.14 <sup>+0.05</sup> <sub>-0.07</sub>	146 <sup>+7</sup> <sub>-4</sub>	4.15 <sup>+0.04</sup> <sub>-0.08</sub>	146 <sup>+7</sup> <sub>-4</sub>	4.15 <sup>+0.05</sup> <sub>-0.07</sub>	
		C	144 <sup>+3</sup> <sub>-7</sub>		150 <sup>+5</sup> <sub>-3</sub>		150 <sup>+5</sup> <sub>-3</sub>		145 <sup>+15</sup> <sub>-0</sub>		
	g-T	P	115 <sup>+40</sup> <sub>-14</sub>	4.50 <sup>+0.25</sup> <sub>-0.48</sub>	166 <sup>+43</sup> <sub>-17</sub>	3.98 <sup>+0.21</sup> <sub>-0.37</sub>	167 <sup>+39</sup> <sub>-21</sub>	3.96 <sup>+0.26</sup> <sub>-0.34</sub>	226 <sup>+20</sup> <sub>-22</sub>	3.45 <sup>+0.30</sup> <sub>-0.09</sub>	
		S	88 <sup>+19</sup> <sub>-3</sub>	4.98 <sup>+0.0</sup> <sub>-0.44</sub> <sup>h</sup>	143 <sup>+41</sup> <sub>-11</sub>	4.15 <sup>+0.20</sup> <sub>-0.42</sub>	145 <sup>+37</sup> <sub>-13</sub>	4.15 <sup>+0.21</sup> <sub>-0.40</sub>	141 <sup>+36</sup> <sub>-6</sub>	4.20 <sup>+0.15</sup> <sub>-0.42</sub>	
		C	95 <sup>+19</sup> <sub>-3</sub>		154 <sup>+25</sup> <sub>-14</sub>		149 <sup>+27</sup> <sub>-9</sub>		139 <sup>+96</sup> <sub>-52h</sub>		
	Gauss	L-T	P	144 <sup>+5</sup> <sub>-7</sub>	4.13 <sup>+0.05</sup> <sub>-0.05</sub>	154 <sup>+5</sup> <sub>-4</sub>	4.12 <sup>+0.05</sup> <sub>-0.04</sub>	154 <sup>+4</sup> <sub>-4</sub>	4.13 <sup>+0.04</sup> <sub>-0.05</sub>	137 <sup>+6</sup> <sub>-3</sub>	4.15 <sup>+0.04</sup> <sub>-0.05</sub>
			S	118 <sup>+32</sup> <sub>-3</sub>	4.17 <sup>+0.06</sup> <sub>-0.07</sub>	147 <sup>+9</sup> <sub>-5</sub>	4.15 <sup>+0.04</sup> <sub>-0.08</sub>	148 <sup>+8</sup> <sub>-5</sub>	4.15 <sup>+0.04</sup> <sub>-0.08</sub>	150 <sup>+7</sup> <sub>-6</sub>	4.14 <sup>+0.05</sup> <sub>-0.07</sub>
			C	145 <sup>+4</sup> <sub>-5</sub>		153 <sup>+3</sup> <sub>-5</sub>		151 <sup>+5</sup> <sub>-3</sub>		141 <sup>+11</sup> <sub>-3</sub>	
M-R		P	134 <sup>+11</sup> <sub>-6</sub>	4.14 <sup>+0.02</sup> <sub>-0.04</sub>	154 <sup>+3</sup> <sub>-4</sub>	4.14 <sup>+0.03</sup> <sub>-0.04</sub>	153 <sup>+4</sup> <sub>-3</sub>	4.14 <sup>+0.03</sup> <sub>-0.04</sub>	145 <sup>+17</sup> <sub>-7h</sub>	4.14 <sup>+0.03</sup> <sub>-0.04</sub>	
		S	148 <sup>+2</sup> <sub>-34</sub> <sup>h</sup>	4.17 <sup>+0.04</sup> <sub>-0.07</sub>	146 <sup>+6</sup> <sub>-3</sub>	4.14 <sup>+0.04</sup> <sub>-0.04</sub>	146 <sup>+6</sup> <sub>-3</sub>	4.15 <sup>+0.02</sup> <sub>-0.05</sub>	146 <sup>+7</sup> <sub>-3</sub>	4.14 <sup>+0.05</sup> <sub>-0.04</sub>	
		C	146 <sup>+2</sup> <sub>-7</sub>		150 <sup>+4</sup> <sub>-2</sub>		150 <sup>+4</sup> <sub>-2</sub>		145 <sup>+13</sup> <sub>-0</sub>		
g-T		P	145 <sup>+5</sup> <sub>-7</sub>	4.13 <sup>+0.05</sup> <sub>-0.05</sub>	154 <sup>+5</sup> <sub>-4</sub>	4.11 <sup>+0.05</sup> <sub>-0.04</sub>	154 <sup>+4</sup> <sub>-4</sub>	4.14 <sup>+0.04</sup> <sub>-0.05</sub>	137 <sup>+19</sup> <sub>-3</sub>	4.15 <sup>+0.04</sup> <sub>-0.08</sub>	
		S	148 <sup>+6</sup> <sub>-32</sub>	4.17 <sup>+0.06</sup> <sub>-0.07</sub>	147 <sup>+8</sup> <sub>-5</sub>	4.15 <sup>+0.04</sup> <sub>-0.08</sub>	147 <sup>+8</sup> <sub>-4</sub>	4.15 <sup>+0.04</sup> <sub>-0.08</sub>	149 <sup>+7</sup> <sub>-5</sub>	4.14 <sup>+0.07</sup> <sub>-0.05</sub>	
		C	146 <sup>+5</sup> <sub>-4</sub>		153 <sup>+3</sup> <sub>-5</sub>		151 <sup>+4</sup> <sub>-3</sub>		141 <sup>+14</sup> <sub>-2</sub>		

<sup>a</sup> Prior on the stellar mass distribution, either flat or Gaussian distribution.

<sup>b</sup> Observables adopted in the solution to constrain the age and the mass of the binary system: L-T: luminosity and temperature; M-R: stellar mass and radius; g-T: surface gravity and temperature.

<sup>c</sup> Solution for the primary (P, Cepheid), secondary (S, red giant), combined (C).

<sup>d</sup> Solution for stellar age (Myr) and stellar mass (solar units) based on evolutionary models with an overshooting parameter  $\beta=0$  (no overshooting) and a mass-loss parameter  $\eta = 0$  (no mass-loss).

<sup>e</sup> Solution based on evolutionary models with  $\beta=0.2$  (mild overshooting) and  $\eta=0$  (no mass-loss).

<sup>f</sup> Solution based on evolutionary models with  $\beta=0.2$  (mild overshooting) and  $\eta=0.4$  (canonical mass-loss rate).

<sup>g</sup> Solution based on evolutionary models with  $\beta=0.2$  (mild overshooting) and  $\eta=4.0$  (enhanced mass-loss rate).

<sup>h</sup> Errors in *italic* indicate that the confidence interval is poorly defined.



TABLE 4  
 BAYES FACTORS FOR THE DIFFERENT SETS OF MODELS AND FOR EITHER A FLAT OR A GAUSSIAN MASS PRIOR.

MP <sup>a</sup>	Obs. <sup>b</sup>	Star <sup>c</sup>	$\beta = 0.0, \eta = 0^d$	$\beta = 0.2, \eta = 0^e$	$\beta = 0.2, \eta = 0.4^f$	$\beta = 0.2, \eta = 4.0^g$	
Flat	L-T	P	0.395	0.393	0.369	0.007	
		S	0.367	0.247	0.255	0.248	
		C	0.145	0.097	0.094	0.002	
	M-R	P	0.014	0.001	0.001	$< 10^{-3}$	
		S	$< 10^{-3}$	0.001	0.001	0.001	
		C	$< 10^{-3}$	$< 10^{-3}$	$< 10^{-3}$	$< 10^{-3}$	
	g-T	P	0.499	0.567	0.534	0.011	
		S	0.236	0.311	0.321	0.304	
			C	0.117	0.177	0.171	0.003
	Gauss	L-T	P	0.654	0.857	0.825	0.002
S			0.128	0.758	0.800	0.844	
C			0.083	0.650	0.660	0.001	
M-R		P	0.159	0.010	0.010	$< 10^{-3}$	
		S	$< 10^{-3}$	0.009	0.010	0.012	
		C	$< 10^{-3}$	$< 10^{-3}$	$< 10^{-3}$	$< 10^{-3}$	
g-T		P	0.704	1.017	1.000	$< 10^{-3}$	
		S	0.042	0.949	1.000	0.978	
			C	0.030	0.965	1.000	$< 10^{-3}$

<sup>a</sup> Prior on the stellar mass distribution, either flat or Gaussian distribution.

<sup>b</sup> Observables adopted in the solution to constrain the age and the mass of the binary system: L-T: luminosity and temperature; M-R: stellar mass and radius; g-T: surface gravity and temperature.

<sup>c</sup> Solution for the primary (P, Cepheid), secondary (S, red giant), combined (C).

<sup>d</sup> Solution for stellar age (Myr) and stellar mass (solar units) based on evolutionary models with an overshooting parameter  $\beta=0$  (no overshooting) and a mass-loss parameter  $\eta = 0$  (no mass-loss).

<sup>e</sup> Solution based on evolutionary models with  $\beta=0.2$  (mild overshooting) and  $\eta=0$  (no mass-loss).

<sup>f</sup> Solution based on evolutionary models with  $\beta=0.2$  (mild overshooting) and  $\eta=0.4$  (canonical mass-loss rate).

<sup>g</sup> Solution based on evolutionary models with  $\beta=0.2$  (mild overshooting) and  $\eta=4.0$  (enhanced mass-loss rate).